OXFORD GENETICS

GENETICS, 2023, 225(2), iyad123
https://doi.org/10.1093/genetics/iyad123
Advance Access Publication Date: 11 July 2023
Investigation

The transcriptional regulator Ume6 is a major driver of early gene expression during gametogenesis

Anthony Harris, Elçin Ünal *

Department of Molecular and Cell Biology, University of California, Berkeley, CA 94720, USA

*Corresponding author: Department of Molecular and Cell Biology, University of California, Berkeley, CA 94720, USA. Email: elcin@berkeley.edu

Abstract

The process of gametogenesis is orchestrated by a dynamic gene expression program, where a vital subset constitutes the early meiotic genes. In budding yeast, the transcription factor Ume6 represses early meiotic gene expression during mitotic growth. However, during the transition from mitotic to meiotic cell fate, early meiotic genes are activated in response to the transcriptional regulator Ime1 through its interaction with Ume6. While it is known that binding of Ime1 to Ume6 promotes early meiotic gene expression, the mechanism of early meiotic gene activation remains elusive. Two competing models have been proposed whereby Ime1 either forms an activator complex with Ume6 or promotes Ume6 degradation. Here, we resolve this controversy. First, we identify the set of genes that are directly regulated by Ume6, including *UME6* itself. While Ume6 protein levels increase in response to Ime1, Ume6 degradation occurs much later in meiosis. Importantly, we found that depletion of Ume6 shortly before meiotic entry is detrimental to early meiotic gene activation and gamete formation, whereas tethering of Ume6 to a heterologous activation domain is sufficient to trigger early meiotic gene expression and produce viable gametes in the absence of Ime1. We conclude that Ime1 and Ume6 form an activator complex. While Ume6 is indispensable for early meiotic gene expression, Ime1 primarily serves as a transactivator for Ume6.

Keywords: meiosis, gametogenesis, transcription, Ime1, Ume6, gene regulation, transcription factor, LUTI, activation domain, GFP nanobody

Introduction

Gametogenesis culminates n the formation of reproductive cells via a series of highly coordinated processes driven by a dynamic and tightly controlled gene expression program. One key process in gametogenesis is meiosis, a specialized form of cell division that involves recombination between homologous chromosomes and reduction of chromosome number by half. Faithful execution of meiosis is crucial, as most human miscarriages and congenital birth defects arise from meiotic errors (Hassold and Hunt 2001; Nagaoka *et al.* 2012). Moreover, inappropriate activation of meiotic genes has been implicated in a range of cancer types, underscoring the significance of proper meiotic gene regulation (Hanahan and Weinberg 2011; McFarlane and Wakeman 2017; Feichtinger and McFarlane 2019; Lingg *et al.* 2022). Therefore, understanding the mechanisms that regulate gene expression and meiotic execution during gametogenesis is of utmost importance.

In the budding yeast *Saccharomyces cerevisiae*, gametogenesis is characterized by the activation of a series of temporally distinct gene expression clusters. The first cluster, known as the early meiotic genes (EMGs), contains evolutionarily conserved meiosis-specific genes required for DNA replication, recombination, and synapsis that ensure proper segregation of chromosomes into gametes. The coordinated expression of EMGs during gametogenesis is achieved through the common upstream regulatory sequence 1 (URS1) motif found in their promoters, which is recognized by the transcription factor Ume6 Park *et al.* 1992). Ume6 interacts with 3 other factors—Sin3, Rpd3, and Ime1—to toggle the expression of EMGs on or off in different developmental contexts (Park *et al.* 1992; Bowdish and Mitchell 1993; Washburn and Esposito 2001). This is achieved through 3 distinct regions in Ume6: the DNA-binding domain, the Sin3-Rpd3 histone deacetylase binding domain, and the Ime1 binding domain. Ume6 coordinates the expression of EMGs by recruiting these factors to EMG promoters.

During mitotic growth, EMGs are repressed by a complex made of Ume6 and Sin3-Rpd3. Ume6-dependent targeting of Sin3-Rpd3 to EMG promoters creates a repressive chromatin state, partly through the deacetylation of histone H4 lysine 5 (Strich *et al.* 1989; Wang *et al.* 1990; Vidal *et al.* 1991; Rundlett *et al.* 1998). In parallel, the *IME1* promoter is strongly repressed by nutritional cues, and any Ime1 protein produced is kept outside the nucleus in a cyclin-dependent kinase (CDK) and target of rapamycin (TOR)-dependent manner (Colomina *et al.* 1999, 2003; van Werven and Amon 2011). These conditions produce cells that cannot enter meiosis and ensure separation between mitotic and meiotic events.

In respirationally competent diploid cells, the *IME1* promoter is derepressed in response to nitrogen and glucose starvation (reviewed in van Werven and Amon 2011). Once translated, Ime1 is phosphorylated by the kinases Rim11 and Rim15 to promote its nuclear localization and interaction with Ume6 (Malathi *et al.* 1997, 1999; Vidan and Mitchell 1997; Pnueli *et al.* 2004). The *IME1* promoter itself contains a URS1 motif, which allows Ime1 to regulate its own expression (Moretto *et al.* 2018). Therefore, the exchange

Received: April 07, 2023. **Accepted:** June 23, 2023

of Sin3-Rpd3 for Ime1 is a key driving force in the stimulation of EMGs and the entry of cells into the meiotic program.

The functional analysis of *UME6* has largely relied on the characterization of a null mutant, *ume6Δ*, which manifests pleiotropic phenotypes and gene expression patterns resulting from constitutive loss of EMG repression (Park *et al.* 1992; Strich *et al.* 1994; Bowdish *et al.* 1995; Williams *et al.* 2002). Therefore, the subset of genes that are directly regulated by Ume6 remains unclear. Furthermore, utilization of this null mutant has made it difficult to assess the meiosis-specific functions of *UME6* and to understand how the interaction between Ume6 and Ime1 influences EMG expression. Consequently, 2 distinct models have been proposed to explain the impact of Ime1 on Ume6 during meiosis. The first model suggests that Ime1, which possesses an activation domain (AD), binds to Ume6 and transforms the complex from a transcriptional repressor into an activator, thereby resulting in EMG expression (Fig. 1 top panel; Rubin-Bejerano *et al.* 1996; Smith *et al.* 1993; Washburn and Esposito 2001; Bowdish *et al.* 1995). Consistent with this model, Raithatha *et al.* found that Ume6 remains bound to EMG promoters when these genes are activated (Raithatha *et al.* 2021). The second model posits that binding of Ime1 to Ume6 serves as a signal that leads to the subsequent degradation of Ume6, thereby releasing EMG repression (Fig. 1, bottom panel; Mallory *et al.* 2007, 2012; Law *et al.* 2014). While the basis of these discordant observations regarding Ume6 stability is not clear, the difference may stem from the asynchrony with which sporulating cultures of *S. cerevisiae* proceed through meiosis.

By using 2 different meiotic synchronization methods, here we describe a thorough mechanistic characterization of Ume6's role in meiotic gene expression. We surprisingly find that Ume6 is upregulated early in meiosis, downstream of Ime1, and is degraded only after prophase I, downstream of the transcriptional regulator Ndt80. Furthermore, by using an inducible protein depletion approach, we identify 144 genes that become derepressed upon acute removal of Ume6 during mitotic growth, thereby revealing its direct transcriptional targets. The expression of the same gene set is hindered when Ume6 is depleted during the transition from mitotic to meiotic cell fate. Thus, we provide conclusive evidence that Ume6 plays a critical role in EMG expression and gamete production, consistent with the coactivator model. This is in contrast with the role of Ume6 during mitotic growth, where our data confirm that it acts primarily as part of a repressive complex. Finally, by using a nanobody-based trap, we found that tethering of a heterologous transactivation domain to Ume6 is sufficient to induce EMGs and produce viable gametes in the absence of Ime1, demonstrating that Ume6 is the primary determinant of EMG targeting. Altogether, our findings highlight Ume6 as an essential meiotic transcription factor, working in concert with Ime1, rather than a mitotic repressor that is simply an antagonist of meiotic gene expression.

Materials and methods

Strains and plasmids

The strains for this study, listed in Supplementary Table 4, are derivatives of the sporulation proficient SK1 strain background (Padmore *et al.* 1991). The following alleles for were derived from other studies: *pCUP-IME1* and *pCUP-IME4* (Berchowitz *et al.* 2013), *pGAL-NDT80* and *GAL4-ER* (Benjamin *et al.* 2003), *HTB1-mCherry* (Matos *et al.* 2008), *GFP-IME1* (Moretto *et al.* 2018), and LexA/*lexO* (Ottoz *et al.* 2014).

Gene tagging or deletion was carried out using a PCR-mediate 1-step integration protocol described previously (Longtine *et al.* 1998; Janke *et al.* 2004) and the PCR products were generated from plasmids in Supplementary Table 5 using primers from Supplementary Table 6.

Endogenous Ume6 was C-terminally tagged with 3 V5 epitopes (3V5) using plasmid pUB81 and Ume6 C-terminal tagging primers. A *UME6* degron allele was generated by C-terminally tagging endogenous Ume6 with an auxin-inducible degron (IAA7) and a 3V5 epitope from plasmid pUB763 using C-terminal tagging primers. To delete the *UME6* gene, the open reading frame (ORF) was replaced by a HygBMX6 marker from plasmid pUB217 using *ume6Δ* primers. A plasmid containing *3V5-αGFP* for Ume6 tagging was generated as follows: a 3v5 polymerase chain reaction (PCR) product from pUB84 was generated using 3v5 fragment primers. Along with this fragment, pUB1707 (gifted from Laura Lackner's Lab) was subjected to *HindIII* and *Sal1* digestion at 37° for 1 h. Enzymatic inactivation was then carried out at 80 °C for 20 min. Digested products were separated by gel electrophoresis on a 1% agarose gel in 1×TBE for 25 min. Fragments were then excised and transferred from the gel to a 1.5 mL Eppendorf tube where they were subjected to clean up using the QIAquick Gel Extraction Kit (QIAGEN) according to protocol. Plasmid was then constructed using an New England BioLabs (NEB) T4 Ligase protocol (NEB—m0202L) and transformed into competent bacteria (DH5α) for amplification. Plasmid was collected using QIAquick Plasmid Kit (QIAGEN) and named pUB2441 (*3V5-αGFP*). To C-terminally tag endogenous Ume6, a *3V5-αGFP* fragment from pUB2441 was generated using Ume6 C-terminal tagging primers.

The LexA/*lexO* system, described previously (Ottoz *et al.* 2014), was exploited to control *OsTIR* expression (*4xlexO-osTIR*). Additionally, to increase *OsTIR* output during meiosis, an *8xlexO-osTIR* was cloned into a *HIS3* single integration vector by Gibson Assembly (Gibson *et al.* 2009). Fragments were generated using pUB817, pUB99, and pUB925, with primers for *OsTIR* Fragment, *HIS* Vector, and *8x-lexO* Fragment. Fragments were then ligated according to the Gibson protocol outlined by NEB to generate plasmid pUB2442. pUB1052 and pUB2442 were digested using *PmeI* at 37 °C for 1 h. Fragments for *lexA-GAL4AD* and *8xlexO-osTIR* were then integrated at the *TRP1* and *HIS3* locus, respectively.

Rescuing of *ime1Δ* using the heterologous AD B112 was achieved by constructing integration plasmids containing the full *IME1* promoter and either tagged or untagged B112. As a vector, pUB969 was amplified with pUB969 Vector Amplification primers. The fragment for *pIME1* was amplified with *pIME1* Fragment primers. Length of the *IME1* promoter was decided using Moretto *et al.* (2018) and ensuring both *IRT1* and *IRT2* (−2314 bp from *IME1* AUG) were included. This was done to recapitulate *IME1* transcriptional regulation and restrict AD expression to meiotic conditions. The fragment for *GFP* was amplified using *GFP* Fragment primers. A fragment for B112 with homology to *GFP* and containing the *SV40 NLS* sequence was amplified using *SV40-NLS-B112 (GFP)* Fragment primers from pUB1054. Plasmids were digested, ligated, and collected as described by the NEB protocol. Sequences were validated by PCR and sequencing and named pUB2443. The plasmid for B112 lacking *GFP* were produced using pUB2443 by first amplifying B112 using primer *SV40-NLS-B112* Fragment primers. Then, parent plasmids and fragments were digested using *XmaI* and *SacI* at 37 °C for 1 h before enzymes were heat inactivated at 80 °C for 20 min. Vector and inserts were then ligated according to the NEB protocol for the T4 ligase reaction before being named pUB2446. Single integration vectors for *IME1* were constructed in a similar way. *IME1* and *GFP-IME1* fragments were amplified from genomic DNA using primer *GFP-IME1* or *IME1* Fragment primers, respectively. Plasmid pUB2443, along with *IME1* and *GFP-IME1* fragments were digested using *XmaI* and *SacI* at 37°C for 1 h before

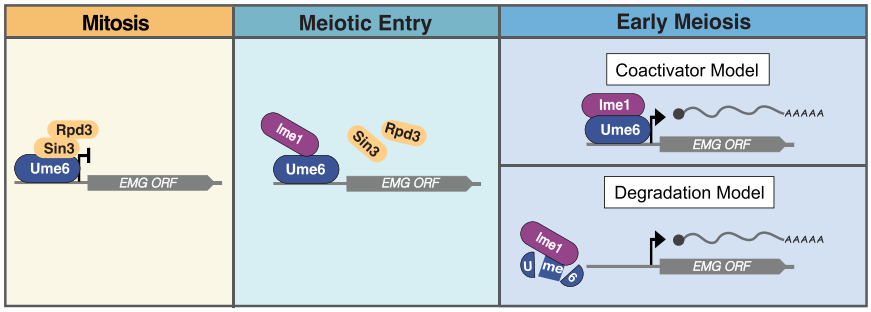

Fig. 1. Two models of EMG expression through Ume6 and Ime1 interaction. During vegetative growth, Ume6 associates with the Sin3-Rpd3 complex ensuring quiescence of the EMGs. The decision to enter meiosis requires exposure to nutrient and mating-type specific cues that help drive many events including: (1) dissociation of Sin3-Rpd3 from Ume6 and (2) expression of the Ime1 transcription factor. Once expressed, Ime1 associates with Ume6. This association is critical to initiating meiotic initiation through EMG expression. However, how Ime1 binding influences Ume6 to promote EMG expression remains unclear. Two models have been presented to explain how Ime1 binding to Ume6 stimulates EMG expression. In the "Coactivator model," Ime1 serves as a transactivator, and its binding converts Ume6 to an activator complex. In the "Degradation model," Ime1 acts as a signal for Ume6 degradation, and its binding displaces Ume6 from EMG promoters.

heat inactivation at 80 °C for 20 min. Fragments were then ligated using T4 Ligase according to the NEB protocol before being named pUB2444 (*pIME1-GFP-linker-IME1-HIS3*) or 2446 (*pIME1-IME1-HIS3*). All plasmids were sequence verified.

Ume6^{T99N} was created using a similar Cas9-based method to a previously published protocol (Sawyer *et al.* 2019). gRNA primers detailed in Supplementary Table 6a were inserted into a centromeric plasmid (pUB1305) carrying a *URA3* marker and *pPGK1-dCas9* to generate pUB2447 and pUB2448. These plasmids were co-transformed into yeast with Ume6^{T99N} Repair Template primers to introduce the missense mutation, T99N (ACT to AAT). The plasmid was sustained on SC-ura plate for selection and successful transformants were then transferred to nutrient rich plates to lose the plasmid.

Growth conditions

Mitotic Ume6 depletion

For mitotic depletion assays, cells with wild-type (WT) *UME6*, *UME6* null allele (*ume6Δ*), and *UME6-AID-3V5; lexA-ER-B112* strains with and without *p4xlexO-OsTIR* were first grown in YPD (1% yeast extract, 2% peptone, 2% dextrose, 22.4 mg/L uracil, and 80 mg/L tryptophan) for ~24 h to reach saturation ($OD_{600} \geq 10$). YPD cultures were then used to inoculate fresh YPD to $OD_{600} = 0.2$ and grown for ~3 h to log phase ($OD_{600} \geq 0.5$). During log phase, a sample for WT and *ume6Δ* was taken. Then, induction of *TIR* was initiated as follows. *UME6-AID; lexA-ER-B112* cells with and without the *p4xlexO-OsTIR* allele had ß-estradiol added (40 nM). Cells were incubated for 30 min before 3-indoleacetic acid (auxin) was added (200 µM). However, Ume6-AID-3v5 depletion only occurred in TIR+ strains. During the time course, samples were collected for RNA and protein extraction at −30 (ß-estradiol addition), 0 (auxin addition), 15, 30, 60, and 120 min.

Meiotic synchronization

A general starvation-based method was used to sporulate cells. Briefly, cells were grown in YPD for ~24 h shaking at 275 rpm to reach saturation ($OD_{600} \geq 10$). The YPD culture was then used to inoculate BYTA (1% yeast extract, 2% bacto tryptone, 1% potassium acetate, and 50 mM potassium phthalate) to $OD_{600} = 0.25$ and grown for 16–18 h at 30 °C to $OD_{600} \geq 5$. These cells were then pelleted, washed with sterile water, and resuspended in sporulation media (SPM; 40 mg Adenine Hemisulfate, 40 mg Uracil, 20 mg Histidine, 20 mg Leucine, 20 mg Tryptophan, 20 g KOAc (2%) 0.02% raffinose, pH 7 in 1 L Arrowhead H_2O) to a density of $OD_{600} = 1.85$ and shaken at 30 °C at 275 rpm for the remainder of the experiment. Sporulation efficiency was always checked under a light microscope ~24 h after shifting to SPM to determine the percentage of tetrads formed. In Figs. 3a–e and 4a–g, *pCUP1-IME1* and *pCUP1-IME4* system was used to synchronize meiotic entry as described previously (Berchowitz *et al.* 2013; Chia and van Werven 2016). The induction timing and expression levels of *IME1* and *IME4* in this context have been previously characterized (Chia and van Werven 2016; Chia *et al.* 2021). Note that the use of *pCUP-IME1 pCUP-IME4* causes a reproducible increase in total expression for many EMGs analyzed at 2.5 h before dropping at 3 h (observable in the heatmaps and individual plots). Cells appear to then equilibrate. The cause of this fluctuation is unclear but has also been observed by other researchers in the lab.

In Fig. 3f–h, *NDT80* Block-Release system was used to synchronize progression into the meiotic divisions as described previously (Benjamin *et al.* 2003; Carlile and Amon 2008). The induction timing and expression level of *NDT80* in this context have been previously characterized (Benjamin *et al.* 2003). After 5 h in SPM, ß-estradiol (1 µM final) was added to induce *NDT80* expression. During the time course, samples were collected for RNA and protein extraction just prior to *NDT80* induction (0 h), and 0.5, 1.0, 1.5, 2.0, 2.5, 3, 3.5, and 4 h following induction.

Meiotic depletion

Strains carrying both *UME6-AID-3V5; lexA-ER-GAL4$^{770–881}$* with and without the *p8xlexO-OsTIR* allele were processed as described in "Meiotic Synchronization" with the following modifications. After 0.5 h in SPM, ß-estradiol (5 nM final) and auxin (200 µM final) were added simultaneously. Ume6-AID-3v5 depletion occurred only in the strain carrying *p8xlexO-OsTIR*. After additional 1.5 h (2 h in SPM), copper (II) sulfate (50 µM final) was added to trigger *IME1* and *IME4* expression from *pCUP1* promoter to release cells into meiotic prophase. Throughout the time course, samples were collected for RNA and protein extraction: after transition to SPM (0.5 h), post Ume6-AID depletion (2 h), and post *IME1* and *IME4* induction (2.5, 3, 4.5, and 6 h). Note that the TIR+ strain used for the meiotic depletion experiments carries 8 *lexO* sites within the osTIR1 promoter and that both TIR+ (Ume6 depletion) and TIR- (control) strains contain the chimeric transcription factor LexA-ER-GAL4$^{770–881}$, instead of LexA-ER-B112, for triggering *osTIR1* expression in the presence of ß-estradiol. Furthermore, lower concentration of ß-estradiol (5 nM vs 40 nM) was used to

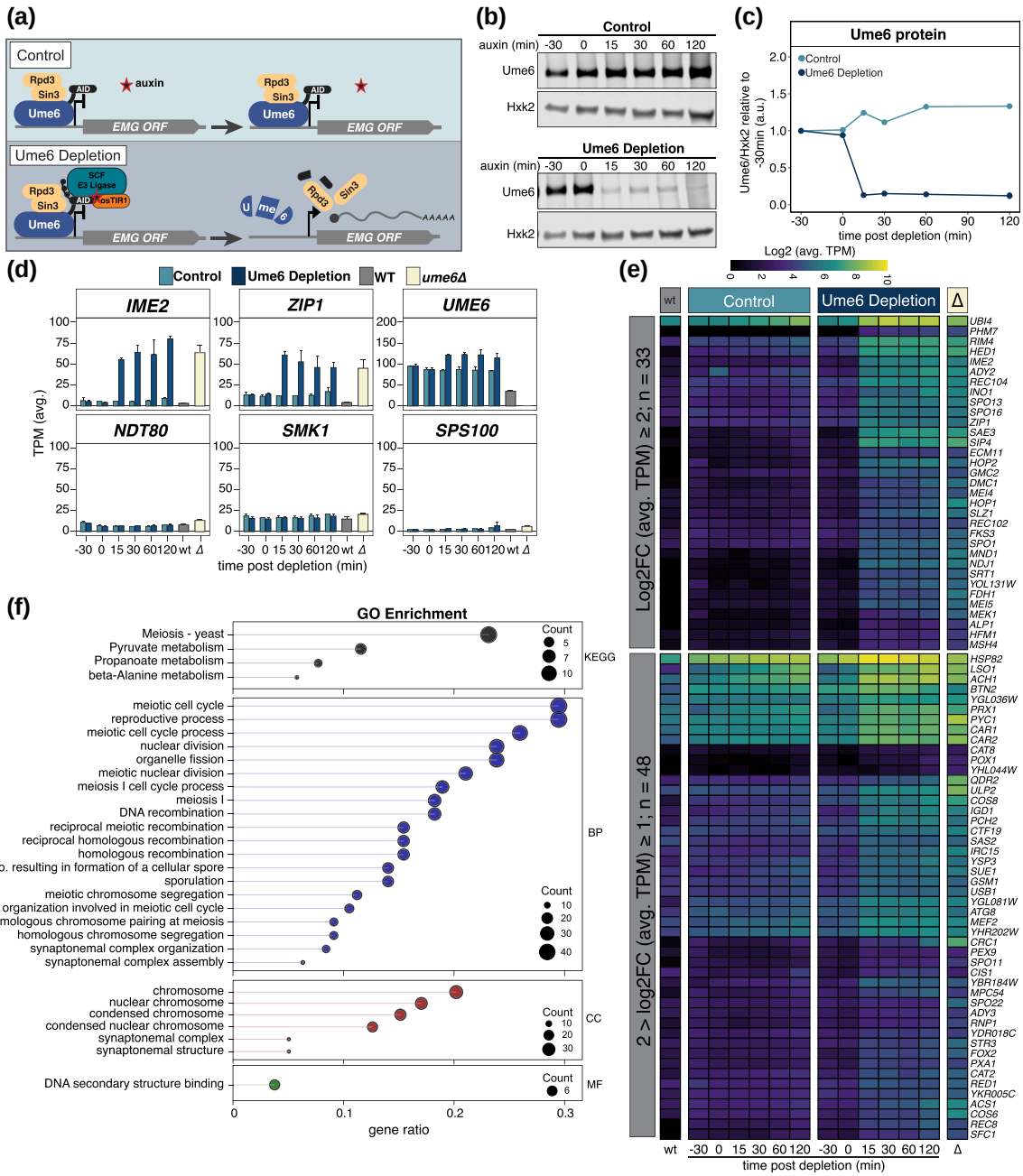

Fig. 2. Acute depletion of Ume6 results in the derepression of EMGs in mitotically dividing cells. a) Illustration of Ume6 depletion scheme using the auxin-inducible degron system. The Ume6-Sin3-Rpd3 repressive complex occupies the EMG promoters. In the absence of *osTIR* (control), the introduction of auxin does not trigger Ume6 degradation and the EMG genes that it regulates remain repressed. Conversely, cells expressing *osTIR* (Ume6 depletion) in the presence of auxin recruit the E3 ligase to the auxin-inducible degron tag associated with Ume6 for poly-ubiquitylation and subsequent degradation of Ume6-AID, which also displaces Sin3-Rpd3. Degradation of Ume6 derepresses EMGs resulting in their expression. Note that *osTIR* is under the control of *lexO* promoter, which can be induced by LexA-ER-B112 (mitotic depletion) or LexA-ER-GAL4$^{770–881}$ (meiotic depletion) upon addition of beta-estradiol. Please refer to *Materials and methods* for further details. b, c) Ume6 protein levels were monitored in response to addition of auxin and beta-estradiol in the presence or absence of *osTIR* (Ume6 depletion or control, respectively). Strains possessing (UB17646) or lacking (UB18287) the *osTIR* construct or strains with WT *UME6* (WT; UB17716) or *ume6Δ* (*ume6Δ*; UB17718) were inoculated in YPD. Cultures were grown overnight to OD_{600} > 10 and then back diluted to OD_{600} = 0.25. Once cells reached log phase (OD_{600} = 0.5), ß-estradiol (40 nM) was added to all cultures (t_{auxin} = −30 min). Cells were allowed to continue shaking for 30 min before auxin (200 µM) was added to all cultures, initiating Ume6-AID degradation only in the *osTIR* containing strains (t_{auxin} = 0 min). Samples for protein and RNA were then collected at the designated time points. Note, cultures for WT *UME6* and *ume6Δ* were collected at t_{auxin} = −30 min prior to chemical treatments. b) Ume6 protein levels were monitored by anti-V5 immunoblotting and using Hxk2 as a loading control. Representative blots from 1 of 3 biological replicates are shown. c) Quantification of immunoblots in (b). To investigate the EMG response to Ume6 degradation, RNA was extracted, and cDNA libraries were generated, sequenced, and analyzed as described in *Materials and methods*. d) Time series data for control and Ume6 depletion are shown as well as for *UME6* and *ume6Δ*. The average TPM for *IME2*, *ZIP1*, *UME6*, *NDT80*, *SMK1*, and *SPS100* are presented with standard error for 3 biological replicates. e) A heatmap as in Supplementary Fig. 1e highlighting a subset of DEGs that showed the greatest response to Ume6 depletion at t = 30 min. This resulted in 33 DEGs with a log2FC ≥ 2 (top) and 48 DEGs with a log2FC ≥ 1 and < 2. f) GO enrichment analysis of the 144 DEGs that responded to Ume6 depletion. The gene ratio is shown on the x-axis and is the percent of genes in a given GO term out of the total 144 genes total. Point size denotes the number of genes in that GO term and color signifies category: KEGG, KEGG pathway database; BP, biological process; CC, cellular component; MF, molecular function.

induce *osTIR* expression. These adjustments were necessary in order to avoid growth and sporulation defects in cells carrying *lexA-ER-GAL4*$^{770–881}$. As a result of these modifications, the extent of Ume6 depletion was less dramatic in meiotic cells compared to mitotic cells. Nevertheless, we still observed significant defects in EMG expression and sporulation efficiency, indicating that meiotic cells are highly sensitive to Ume6 levels.

Immunoblotting

For protein extraction from meiotic cultures, ~3.7 OD_{600} of cells were collected and resuspended in 5% TCA (w/v). For mitotic cultures, ~ 1 OD_{600} of cells were collected. Samples were processed by centrifugation (1900×g, 3 m, room temperature) and washed in TE50, pH 7.5 (50 mM Tris and 1 mM EDTA) and acetone before being dried overnight at room temperature. Pellets were resuspended in protein breakage buffer [TE50, 2.75 mM dithiothreitol (DTT) supplemented with 1× cOmplete EDTA-free protease inhibitor cocktail (Roche)] and disrupted using a Mini-Beadbeater-96 (BioSpec). Lysates were then mixed with 50 µL of 3xSDS loading buffer (187.5 mM Tris, pH 6.8, 6% 2-mercaptoethanol, 30% glycerol, 9% SDS, and 0.05% bromophenol blue), incubated at 95 °C for 5 min to denature, and allowed to cool for at least 5 min before centrifugation at full speed for 5 min.

Proteins were separated by SDS-PAGE electrophoresis on a Bolt 4–12% Bis-Tris Plus Gel (Thermo Fisher Scientific) and then transferred onto a 0.45-µm nitrocellulose membrane in a Mini Trans-Blot Cell (Bio-Rad) containing 25 mM Tris, 192 mM glycine, and 7.5% methanol. Protein transfer was carried out using a Mini Trans-Blot Cell at a constant 180 mA (maximum, 70 V) for 3 h. Membranes were blocked at room temperature for 30 m using Odyssey Blocking Buffer (PBS; LI-COR Biosciences) before being incubated at 4 °C in Odyssey Blocking Buffer (PBS) containing mouse anti-V5 antibody (RRID: AB 2556564, R960-25; Thermo Fisher Scientific) at a 1:3,000 dilution for detection of 3v5 tagged alleles of Ume6. Additionally, hexokinase Hxk2 was used as a loading control and detected using a rabbit anti-Hxk2 antibody (RRID: AB 219918, 1004159; Rockland) at a 1:10,000 dilution. Membranes were incubated at 4 °C for 16–18 h and primary antibody was removed. Membranes were then washed 3 times in 1× PBS (+0.01% Tween) shaking gently for 5 min at room temperature before being placed in the Odyssey Blocking Buffer (PBS) containing antimouse secondary antibody conjugated to IRDye 800CW at a 1:15,000 dilution (RRID: AB 621847, 926-32212; LI-COR Biosciences) and an antirabbit antibody conjugated to IRDye 680RD at a 1:15,000 dilution (RRID: AB 10956166, 926-68071; LI-COR Biosciences). Blots were washed again in PBS (+0.01% Tween-20) as before and imaged with an Odyssey CLx scanner (LI-COR Biosciences). Band intensities were quantified with the Image Studio software associated with the scanner.

Live-cell imaging

Using CellASIC ONIX Microfluidic Platform (EMD Millipore), sporulating cultures (OD_{600} = 1.85) were sonicated briefly to avoid clumping and transferred to a microfluidic Y04D plate and loaded into chambers using a pressure of 8 psi for 5 s. Subsequently, freshly conditioned SPM (filter-sterilized SPM from a meiotic culture at 30 °C 5 h into sporulation) was fed at a flow rate pressure of 2 psi for 24 h (King *et al.* 2019, 2022). The microfluidic Y04E plate was then loaded into an environmental chamber heated to 30 °C mounted on a DeltaVision Elite wide-field fluorescence microscope (GE Healthcare) with a PCO Edge sCMOS camera and operated by the associated softWoRx software. Images were acquired at 60×/1.5116n oil immersion Plan Apochromat objective at 30 min intervals across 21.5 h. An image stack of 4 Z positions at a 1 µm step size were acquired using mCherry (10% Intensity; 25-ms exposure) and FITC (10% Intensity; 25-ms exposure) filter sets. These images were deconvolved in softWoRx software (GE Healthcare) with a 3D iterative constrained deconvolution algorithm (enhanced ratio) with 15 iterations. Once images were collected, Fiji was used to adjust brightness and contrast after images were stabilized with the Image Stabilizer plugin (Li 2008; Schindelin *et al.* 2012).

Quantitative reverse transcription-PCR

For meiotic cultures, OD_{600} ~3.7 of cells were collected. These samples were processed for total RNA first by centrifugation (2 m, 1900g, 4 °C). Supernatant was removed and cells were washed in nuclease-free water before being centrifuged again (1 min, 21,000 g, 4 °C). Water was removed from cell pellet and total RNA was isolated by combining acid-washed glass beads (Sigma Aldrich—G8772), 400 µL TES buffer (10 mM Tris pH 7.5, 10 mM EDTA, 0.5% SDS), and 400 µL acid phenol (0.1% w/v 8-hydroxyquinoline). The solution was shaken in a thermo mixer for 30 m at 65 °C at 1400 rpm and centrifuged (10 min, 21,000 g, 4 °C). Roughly 325 µL of aqueous layer was transferred to 300 µL of chloroform and centrifuged (5 min, 21,000 g, room temperature). Next, 250 µL of the aqueous layer was transferred to 400 µL of 100% isopropanol (supplemented w/50 µL 3 M NaOAc), inverted ~10 times, and incubated for 16–18 h at 4 °C. RNA was then pelleted by centrifugation (20 min, 21,000 g, 4 °C) and washed in 80% EtOH. The EtOH was removed, and pellets were dried for 30–40 min before being resuspended in nuclease-free water. 5 µg of purified total RNA was then treated with DNase (TURBO DNA-free kit, Thermo Fisher, MA, USA) according to manufacturer, and 4 µL (<1 µg) of DNase treated total RNA was then reverse transcribed into cDNA with the use of random hexamers (Superscript III Supermix, Thermo Fisher) according to manufacturer's instructions. cDNA was then quantified using the SYBR green mix (Life Technologies, CA, USA) and measured using the Applied Biosystem StepOnePlus Real-Time PCR system (Thermofisher—4376600). Signal for *IME2*, *NDT80*, *SPO13*, and *UME6* was measured using oligonucleotides outlined in Supplementary Table 6b. Signal was then normalized to *PFY1* for meiotic cultures.

Chromatin immunoprecipitation

For chromatin immunoprecipitation (ChIP), meiotic culture (OD_{600} = ~ 50) was fixed in 1.0% v/v formaldehyde for ~20 min at room temperature before quenching the reaction with 100 mM glycine. Cell pellets were collected by centrifugation (3000×g, 5 min, 4 °C) and washed in cold PBS. Cell pellets were then resuspended in 1 mL FA lysis buffer (50 mM Hepes pH 7.5, 150 mM NaCl, 1 mM EDTA, 1% Triton, 0.1% sodium deoxycholate) with 0.1% sodium dodecyl sulfate (SDS) and 10% w/v cOmplete protease inhibitor pellet. Cells were broken using a mini beadbeater (BioSpec) and lysate was transferred to a 1.5 mL low adhesion Eppendorf tube and debris was cleared by centrifugation (2000×g, 3 min, 4 °C). Supernatant was transferred to a new 1.5 mL low adhesion Eppendorf tube, and lysate was centrifuged (20,000×g, 15 min, 4 °C). Supernatant was discarded, leaving a cloudy pellet behind. Pellets were resuspended in 1 mL lysis buffer + 0.1% SDS + complete protease inhibitor and chromatin was sheared by sonication using a Bioruptor Diagenode (Seraing, Belgium), 8 cycles of 30 s ON/45 s OFF]. From sonicated samples, 50 µL of input was transferred for a 1.5 mL Eppendorf tube. Remaining extracts were incubated overnight at 4 °C in agarose

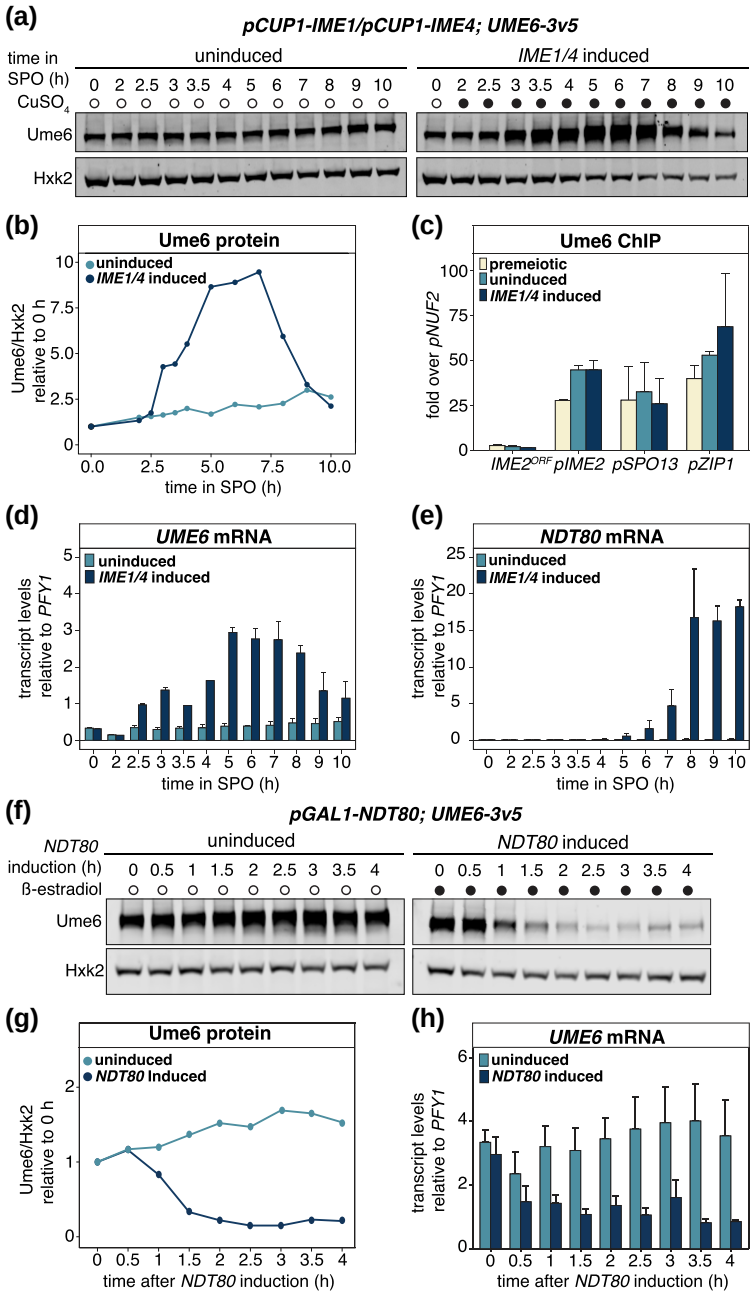

Fig. 3. Changes in *UME6* expression in response to *IME1*/4 and *NDT80* induction. a) Ume6 protein abundance in response to withholding (uninduced) or inducing (induced) *IME1*/4 during synchronous meiotic progression. The strain carrying *pCUP1-IME1* and *pCUP1-IME4* along with a 3v5-tagged allele of *UME6* (UB3301) was transferred to SPM at 0 h, and cells were arrested at meiotic entry. After 2 h, the meiotic culture was split in 2. The vehicle control (water) was added to the first flask preventing meiotic entry. $CuSO_4$ (50 µM) was added to the other flask to induce meiosis. Cells were collected at the indicated times for protein extraction, and Ume6 levels were determined using anti-V5 immunoblotting and Hxk2 as a loading control. Representative blots from 1 of 3 biological replicates are shown. b) Quantification of immunoblotting in a). c) Ume6 occupancy at the *IME2*, *SPO13*, and *ZIP1* promoters, as well as the *IME2 ORF* where binding is not expected was analyzed by ChIP-qPCR in strain UB3301. Cells were transferred to SPM and arrested at meiotic entry by withholding *IME1*/4 for 2 h (premeiotic). At this time, a sample of $OD_{600} = 50$ was collected. *IME1*/4 was then either induced by addition of $CuSO_4$ (50 µM; *IME1*/4 induced) or withheld (uninduced). Cells were allowed to continue in SPM for 2 h after this, and samples of $OD_{600} = 50$ for uninduced and *IME1*/4 induced were collected. Mean enrichment for 3 biological replicates is presented with the standard error of each primer pair used. Ume6 signal at target sites was normalized over *NUF2* promoter enrichment. In addition to protein, RNA samples were collected at the indicated times to monitor expression patterns for d) *UME6* and e) *NDT80* in response to *IME1*/4 induction. RNA was extracted from samples, and transcript levels for *UME6* and *NDT80* were determined using RT-qPCR. The CT mean for 2 biological replicates is presented along with the range for uninduced and *IME1*/4 induced samples at the specified time points. To control for technical variation, we normalized expression of *UME6* and *NDT80* relative to *PFY1*. f) Ume6 protein levels in monitored in response to *NDT80* induction. The strain harboring the *pGAL1-NDT80* and *GAL4-ER* in combination with 3v5-tagged Ume6 (UB21877) was transferred to SPM. Cells were allowed to progress through meiosis for 5 h before arresting at pachytene of prophase I (t = 0 h). A sample for protein and RNA was collected and cultures were split into 2 flasks. The first flask received the vehicle control (EtOH) to withhold *NDT80* expression (uninduced), while the other flask received ß-estradiol (1 µM) to induce *NDT80* expression allowing exit from prophase (*NDT80* induced). Samples were collected at the designated time points. Ume6 levels were determined using anti-V5 immunoblotting and Hxk2 for a loading control as before. Representative blots from 1 of 3 biological replicates are shown. g) Quantification of immunoblots in f). h) *UME6* transcripts in the presence and absence of *NDT80* were monitored by RT-qPCR after RNA extraction. The CT mean of 3 biological replicates is presented along with the standard error. Technical variation was controlled for by normalization to *PFY1*.

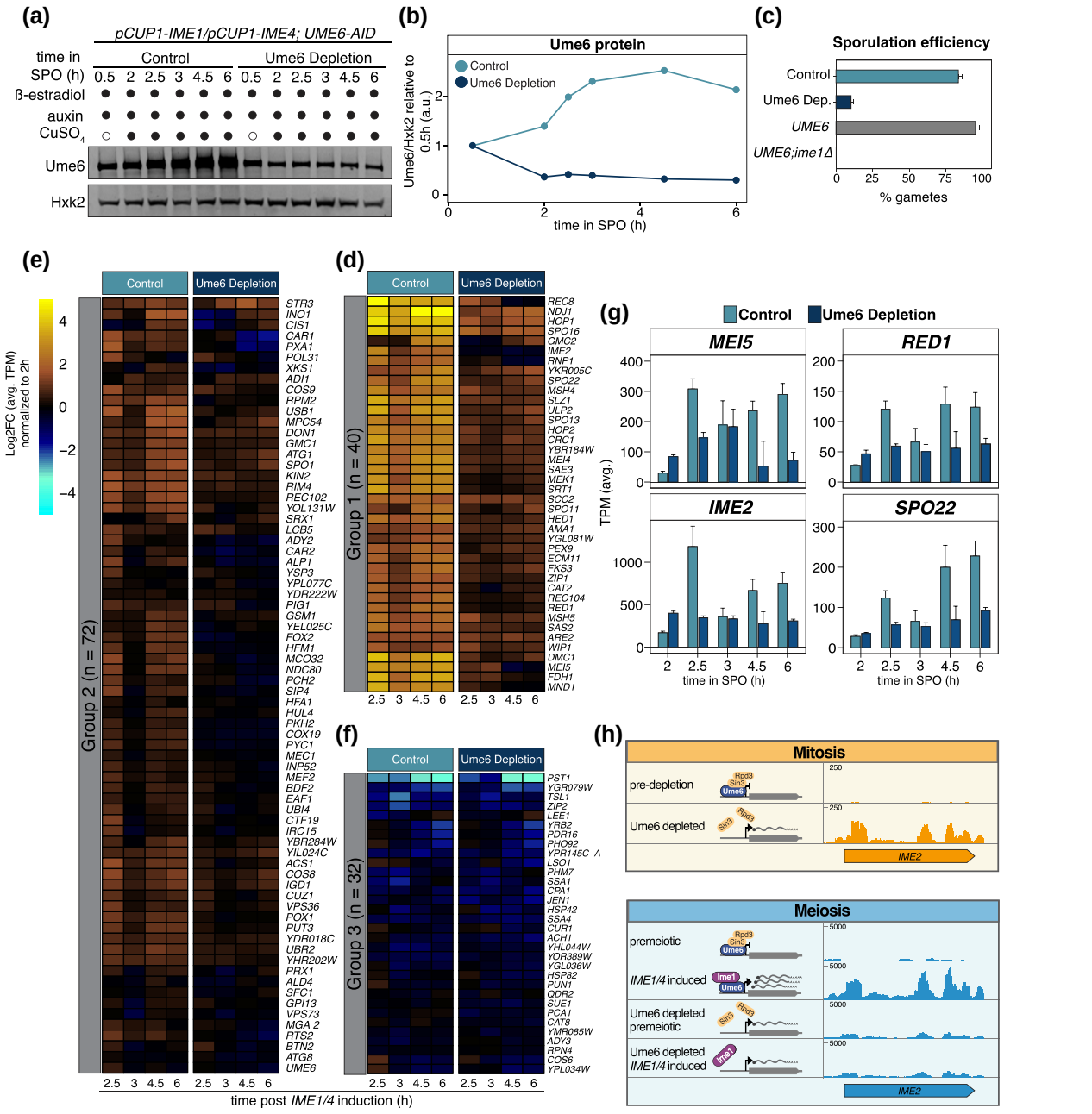

Fig. 4. Ume6 depletion shortly before meiotic entry disrupts gamete formation and EMG expression. Cultures from control (UB25688) and Ume6 depletion (UB25092) strains were transferred to SPM at 0 h. ß-estradiol (5 nM) and auxin (200 μM) were added at 0.5 h. Then, $CuSO_4$ (50 μM) was added at 2 h to induce meiosis. Samples for protein and RNA were collected at designated times. a) Ume6 protein abundance was analyzed using anti-V5 immunoblotting and Hxk2 as a loading control. Representative blots from 1 of 3 biological replicates are shown. b) Quantification of the immunoblots in (a). c) Sporulation efficiency data for control (UB25688) and Ume6 depletion strains (UB25092) along with 2 additional controls, a *pCUP1-IME1*; *pCUP1-IME4*; *UME6* (*UME6*) strain (UB19103) and *ime1Δ* (UB19105) strain. Cells were allowed to complete meiosis for 24 h before calculating sporulation efficiency. For this, 100 cells were counted, and percentage of cells that formed tetrads was noted as % gametes. Data from average of 3 biological replicates is presented for control, Ume6 depletion, *UME6*, and *ime1Δ*. Error bars indicate standard error. d–f) The log2FC of average TPM for 3 biological replicates is shown for the 144 Ume6 targets identified from mitotic cells. To evaluate EMG response to Ume6 degradation following *IME1*/4 induction, TPM were normalized to the 2 h time point just before *IME1*/4 induction. A heatmap of the 144 Ume6 targets shown in Figure S3B was split using k-means clustering based on their Euclidean distance and application of the "elbow test" to identify an optimal k of 3 (k-means = 3). This produced 3 distinct groupings of genes based on their response to *IME1*/4 induction: group 1 (d), group 2 (e), and group 3 (f). g) Four genes from group 1 were selected for closer inspection. This included *MEI5*, *IME2*, *RED1*, and *SPO22*, which are presented as a bar plot showing mean of TPM including the standard error for 3 biological replicates. This bar plot compares control and Ume6 depletion conditions at the designated times. h and i) Genome browser views of mRNA tracks highlighting consequential differences between depleting Ume6 during mitotic growth compared to meiosis for the EMG *IME2*. h) During mitotic growth, prior to Ume6 depletion (predepletion) *IME2* signal is mostly undetectable (top). Then, in response to Ume6 depletion (Ume6 depleted) *IME2* signal appears indicating a loss of repression. i) Conversely, in the presence of Ume6 without Ime1 (premeiotic), signal for *IME2* is mostly undetectable, similar to mitotic conditions, and after *IME1*/4 induction (*IME1*/4 induced), *IME2* becomes strongly expressed as indicated by the mapped reads. However, in the absence of Ume6, before or after *IME1*/4 induction (Ume6 depleted + premeiotic and Ume6 depleted + *IME1*/4 induced, respectively), *IME2* signal remains slightly stronger than premeiotic but much weaker than *IME1*/4 induced. Scales for the genome browser under each condition, mitosis and meiosis, are indicated and an illustration for Ume6's presence and interaction with its cofactors is provided. Scales on the y-axis show relative track heights between mitosis and meiosis.

beads conjugated to anti-V5 antibody (Millipore Sigma—A7345). Bead bound chromatin was then washed twice in 1 mL lysis buffer, buffer 1 (250 mM NaCl in lysis buffer + 0.1% SDS), and finally buffer 2 (10 mM Tris pH 8, 250 mM LiCl, 0.5% NP-40, 0.5% deoxycholate sodium, 1 mM EDTA) before reverse crosslinking was done in Tris-EDTA buffer (100 mM Tris pH 8.0, 10 mM EDTA, 1.0% v/v SDS) at 65 °C overnight. Previously collected inputs were also incubated overnight at 65 °C in Tris-EDTA. After 1 h of proteinase K treatment at 65 °C, samples were cleaned using QiaQuick PCR cleanup (Qiagen—28106) and enrichment of Ume6 at *IME2*, *SPO13*, and *ZIP1*, promoters as well as the *IME2 ORF* was measured by real-time PCR using SYBR green mix. RT-qPCRwas carried out as follows: each IP was run alongside a dilution series of its sample matched input. This was done using primers that target the promoter of *NUF2* (*pNUF2*) as well as the above-mentioned sites. Using the input data, a dilution curve was used to normalize for fragment abundance. Then, Ume6 binding enrichment was assessed looking at the ratio of *pIME2*, *pSPO13*, *pZIP1*, and *IME2 ORF* fragments, over *pNUF2* fragments where Ume6 is not expected to bind. Oligonucleotide sequences used for ChIP are outlined in Supplementary Table 6b.

RNA-seq

RNA samples were collected and processed as described in RT-qPCR section. To prepare mRNA-seq libraries, 10 µg of total RNA was polyA-selected and processed using the NEXTFLEX Rapid Direction RNA-seq Kit (NOVA-5138-10 and NOVA-5138-11; PerkinElmer) according to the provided manual. Quantification of resulting cDNA yields was performed using a Qubit 3 (ThermoFisher Scientific) using the high sensitivity DNA assay kit. AMPure XP beads (A63881; Beckman Coulter) were using during size selection (200–500 bp) and fragment quality and quantity was analyzed using high sensitivity D1000 ScreenTapes on the Agilent 4200 TapeStation (Agilent Technologies, Inc.). Samples were sequenced through the Vincent J. Coates QB3 Genomics Sequencing Facility at the University of California, Berkeley using 100 bp single-end sequencing on an Illumina Novaseq 6000. Alignment of sequenced reads was carried out using either HISAT2 or Kallisto. For HISAT2, the protocol outlined by Pertea *et al.* (2016) was used with SK1 reference genome, sourced from the Saccharomyces Genome Resequencing Project at the Sanger Institute to visualize transcript isoforms (Pertea *et al.* 2016). For Kallisto, pseudoalignments were carried out according to a manual developed by Bray *et al.* to generate transcripts per million reads (TPM) and raw counts tables (Bray *et al.* 2016). Kallisto quant settings were adjusted to -b 5 -l 160 -s 20-single-threads 4 based on fragment lengths determined by the Agilent 4200 TapeStation (Agilent Technologies, Inc.).

Heatmaps and plots

R was further used for Spearman's correlation and with the packages pheatmap (ver. 1.0.12) and ggplot2 (ver. 3.4.0) to generate heatmaps and plots used in this manuscript, respectively (Wickham *et al.* 2019; R Core Team 2021).

Differential gene expression analysis

Identification of differentially expressed genes (DEGs) responsive to Ume6 mitotic depletion was performed using 2 complementary approaches in R (R: ver. 4.1.3; RStudio: ver. 2022.07.1 Build 554). First, raw counts generated from Kallisto were exported to R. Then, using the DESeq2 package (ver. 1.34.0), differences in expression between control and Ume6 depletion samples across time (t = 0, 15, 30, 60, 120 min) were determined using an FDR of 5% (R Core Team; Love *et al.* 2014). To set up time series analysis, the DESeq2 "test" parameter was set to "Likelihood Ratio Test" that, by default, uses the Wald test to generate results tables. Time series analysis between control and Ume6 depletion conditions using DESeq2 identified 177 Ume6-responsive genes (Supplementary Table 1). Depletion of Ume6 during mitotic growth should derepress its targets; therefore, we inspected the list of 177 Ume6-responsive genes looking for sustained derepression from 15 to 120 min (post-Ume6 depletion). We noted some genes that were largely unchanged post-Ume6 depletion (i.e. *ERO1* and *BOI1*, ~1% and ~3% increase, respectively, comparing Ume6 depletion to control at t = 15 min) that were counted significant by DESeq2. Thus, to control for any false positives in our list of 177, we generated a custom R script to filter out these transcripts. In brief, to avoid transcripts that displayed a response independent of Ume6 depletion, we performed pairwise analysis using DESeq2 at t = −30 and 0 min. Those genes with differential expression at these times [Padj < 0.05; abs(log2FC) > 1] were removed. Next, we looked transcripts that displayed an acute response to Ume6 depletion at 15 min [Padj < 0.05 abs(log2FC) > 0.3], as would be expected of direct regulation by Ume6. Filtering of transcripts using this script reduced the list from 177 to 135.

Second, we noted that some genes previously identified in Williams *et al.* 2002 as being derepressed in *ume6Δ* were not present in the list of 177 (i.e. *PIG1*). Further inspection in our TPM table revealed *PIG1* did experience a ~34% increase in expression post-Ume6 depletion (t = 15 min, comparing Ume6 depletion to control). Thus, to identify any genes missed by DESeq2, we performed additional analysis using TPM data and a custom R script. Briefly, we took the ratio between Ume6 depletion and control samples at each time point (t = 15, 30, 60, and 120 min). This was done for the TPM of all genes. Next, we took the average (avg.) of these ratios across all time points. We then looked for genes whose avg. TPM ratio between Ume6 depletion and control across time was ≥1.4 or ≤0.6. Doing so, we identified 128 genes, 98 that were previously called significant by DESeq2. The 30 additional genes were inspected before being added to the list of 135 DESeq2 targets resulting in a total list of 165. Thus, between DESeq2 and TPM analysis we identified 165 distinct genes that responded to Ume6 depletion, referred to herein as our "composite list" (Supplementary Table 1).

ChIP peak curation

Using a previously published dataset from Tresenrider *et al.* (2021) we analyzed ChIP peak scores for our composite list of 165 Ume6 targets. We divided the average ChIP peak score ($n = 3$ biological replicates) for each of the 165 Ume6-responsive genes by the ChIP peak score of *IME2*, a well-characterized Ume6 target and selected those with ratios ≥0.5. This analysis resulted in 144 Ume6-responsive genes that were also enriched for a Ume6 ChIP peak, indicating direct targets (Supplementary Fig. 1e and Supplementary Table 1).

Gene ontology enrichment

Gene ontology (GO) enrichment was performed in R using the clusterProfiler package (Yu *et al.* 2012) together with the org.Sc.sgd.db (ver. 3.14.0; Carlson 2021).

Motif discovery

Motif enrichment analysis for Ume6 targets was performed using Multiple Em for Motif Elicitation (MEME; ver. 5.5.1) (Bailey *et al.* 2015). Sequences for 1,000 bp up- or downstream as well as the ORF were obtained using YeastMine (Balakrishnan *et al.* 2012)

and exported to MEME as Fasta files for analysis with restricting the motif length's upper limit to 15 nucleotides, but otherwise using default settings. A $P < 0.05$ for a motif in a given gene was considered significant. These motifs were also validated using ChIP-Seq data from Tresenrider *et al.* (2021).

Gene set enrichment analysis

Normalized counts generated from DESeq2 were compared between samples using gene set enrichment analysis (GSEA) v4.3.2 (build: 13) to assess enrichment of gene sets (Mootha *et al.* 2003; Subramanian *et al.* 2005). The "EMG" set was generated by analyzing previously established data (Brar *et al.* 2012; Chia *et al.* 2021; Tresenrider *et al.* 2021). First, genes whose TPM changed in response to *pCUP1-IME1 pCUP1-IME4* induction by a log2FC > 1.0 were taken from Tresenrider *et al* (609 genes). Next, using a list of *NDT80* targets generated in Cheng and Otto *et al*, we removed MMGs from this list. The remaining 518 genes were then curated using Brar *et al.* and Chia *et al.*, limiting expression timing to between meiotic entry and prior to metaphase I. Finally, genes with high TPM levels during mitotic growth were also excluded. This resulted in a list of 272 early expressed meiotic genes termed "EMGs". As mentioned, the second set of genes termed "Middle Meiotic Genes" was defined in Cheng *et al.* and Otto *et al.* as a set of 394 genes responsive to *NDT80* induction (*NDT80* cluster, Cheng *et al.* 2018). The desktop version of GSEA was used to load in data and determine enrichment with the following modifications: "Collapse/Remap to gene symbols" was set to "No Collapse" and "Permutation Type" was set to "Gene Set," other settings were unchanged.

Results

Inducible depletion of Ume6 prevents the pleiotropic phenotypes associated with constitutive loss of *UME6* function

In mitotically dividing cells, Ume6 acts as part of a repressive complex leading to the silencing of EMGs (Strich *et al.* 1994; Williams *et al.* 2002). Attempts to understand Ume6's role during mitotic growth have revealed hundreds of genes involved in both meiotic and metabolic functions (Park *et al.* 1992; Strich *et al.* 1994; Bowdish *et al.* 1995; Williams *et al.* 2002). However, these studies primarily relied on the use of a null mutant, *ume6Δ*, which has prolonged exposure to meiosis-specific machinery during the mitotic cell cycle, rendering it extremely sick (Supplementary Fig. 1a) and possibly leading to indirect effects in gene expression.

To overcome the limitations exerted by constitutive loss of *UME6* function, we utilized the auxin inducible degron system (AID, Nishimura *et al.* 2009), which enables rapid depletion of Ume6 carrying an AID tag (Ume6-AID) in response to the plant hormone auxin and the F-box receptor OsTIR1, which is induced by a ß-estradiol activatable transcription factor (Fig. 2a; see *Material and methods* for technical details). Cells carrying the *UME6-AID* allele grew similarly to WT in the absence of auxin and ß-estradiol, suggesting that degron tagging of *UME6* at the endogenous locus does not interfere with its function (Supplementary Fig. 1a).

To test the effectiveness of the *UME6-AID* system, we compared Ume6 levels by immunoblotting in the absence or presence of the F-box receptor OsTIR1 (from here on referred to as "control" and "Ume6 depletion", respectively). In control cells, addition of ß-estradiol and auxin had no detectable influence on Ume6 levels (Fig. 2b and c). In contrast, the same drug regimen resulted in the rapid depletion of Ume6 in cells carrying the F-box receptor (Fig. 2b and c). Ume6 abundance was reduced to ~13% of the initial levels within 15 min and remained low afterwards (Fig. 2b and c).

To measure the transcriptomic response to Ume6 depletion, we performed RNA-seq. We initially analyzed global changes in gene expression by pairwise comparison using Spearman's rank correlation coefficient (ρ; Supplementary Fig. 1b). We found that control and Ume6 depletion samples were initially very similar to one another (−30 min; ρ = 0.995). The correlation decreased, albeit slightly, following induction of Ume6 depletion (ρ = 0.978, 0.982, 0.984, and 0.984 for 15, 30, 60, and 120 min, respectively). This is perhaps not surprising given that even in the case of the *ume6Δ*, global differences in transcript levels were relatively subtle compared to WT (ρ = 0.917). We additionally monitored sample-to-sample variation across time points using principal component analysis (PCA; Supplementary Fig. 1c). PC1 (58%) and PC2 (17%) accounted for 75% of the variation. Initially (−30 min), control and Ume6 depletion samples formed a distinct group, highlighting sample relatedness. After treatment with ß-estradiol and auxin, control and Ume6 depletion samples separated, with control samples only slightly shifting away from 0 min along PC1 and Ume6 depletion samples spreading along PC1 and PC2. Altogether, these transcriptome-wide comparisons indicate that gene expression patterns diverge only after induction of Ume6 depletion, thereby corroborating the temporally controlled nature of the AID system.

We next focused on the expression patterns of a subset of meiotic genes. First, we analyzed *IME2* and *ZIP1*, 2 well-characterized EMGs known to be repressed by Ume6 during mitotic growth (Fig. 2d; Mitchell 1994). In the control strain where Ume6 protein levels remained high, we observed no noticeable change in either *IME2* or *ZIP1* expression relative to WT across all time points. However, upon Ume6 depletion, we observed a 10- and 5-fold upregulation for *IME2* and *ZIP1*, respectively (Fig. 2d, 15 min). *IME2* and *ZIP1* transcripts reached similar levels to that of *ume6Δ* mutant following Ume6 depletion. Furthermore, Ume6 depletion did not affect the expression of mid meiotic (e.g. *NDT80*, *SMK1*) or late meiotic (e.g. *SPS100*) genes (Fig. 2d). Together, these data suggest that the *UME6-AID* system can specifically cause derepression of EMGs in mitotic cells. Finally, we noticed reproducible upregulation of *UME6* transcripts in response to Ume6 depletion (~30% increase between control and Ume6 depletion, Fig. 2d), suggesting that Ume6 autoregulates its own expression.

Mitotic depletion of Ume6 enables the identification of its direct targets

We next identified DEGs responsive to acute Ume6 depletion using 2 complementary approaches (see *Materials and methods* for details). This analysis resulted in a composite list of 165 Ume6-responsive genes (Supplementary Fig. 1d and Supplementary Table 1). This list of targets was further curated using a previously published Ume6 ChIP-Seq dataset, which was acquired in the absence of *IME1* expression when Ume6 should be bound to its targets (Tresenrider *et al.* 2021). This resulted in 144 Ume6-responsive genes that were also enriched for a Ume6 ChIP peak, indicating direct targets (Supplementary Fig. 1e and Supplementary Table 1; Tresenrider *et al.* 2021). To corroborate these results, we employed Multiple EM for Motif Elicitation (MEME) analysis to look for common motifs within or adjacent to the gene bodies of the 144 Ume6-responsive genes (Bailey and Elkan 1994; Bailey *et al.* 2015). MEME identified the core URS1 sequence (5′-GGCGGC-3) in 119 of the 144 genes (83%; Supplementary Fig. 1f). Further inspection of the Ume6 depletion samples revealed that all of the 144 genes were derepressed

rapidly, within 15 min following auxin administration, with 58% (83/144) having a log2FC ≥ 1. Additionally, 56% (81/144) maintained a log2FC ≥ 1 at 30 min indicating a sustained expression (Fig. 2e, Supplementary Table 1). In conclusion, this comparative analysis enabled the identification of a refined gene set that is directly regulated by Ume6.

Many of the Ume6 targets identified in this study are transcriptionally regulated during meiosis (Brar *et al.* 2012; Tresenrider *et al.* 2021). Brar *et al.* (2012) has rigorously categorized the dynamic changes in gene expression with respect to the chronology of meiotic events. Using this dataset, we determined when the Ume6 targets were expressed during meiosis. Doing so, we found that a majority reached their highest expression during meiotic entry (49/144; 34%), DNA replication (12/144; 8%), and recombination (66/144; 46%). This indicates that 88% (127/144) of our Ume6 targets are EMGs. The remaining 12% (17/144) were expressed throughout meiosis, but expression did not peak until mid and late meiosis suggesting additional possible layers of regulation. GO enrichment analysis for the 144 Ume6 targets was largely composed of genes involved in meiotic machinery and metabolism (Fig. 2f). However, other functional classes were also revealed, including protein synthesis, trafficking, RNA processing, and cell wall maintenance. Finally, 18 genes of unknown function were present, and it is possible these genes are involved in one of the abovementioned functions that Ume6 regulates. Altogether, the comparison to the published dataset from Brar *et al.* confirms that the targets identified by the *UME6-AID* system represent meiotically expressed genes.

Mitotic depletion of Ume6 derepresses meiotically expressed LUTIs

A pervasive mechanism of gene regulation has recently been characterized in meiosis, whereby expression of a long undecoded transcript isoform (LUTI) from a distal gene promoter causes downregulation of the canonical, protein-coding transcript from the proximal promoter through the combined act of transcriptional and translational interference (Chen *et al.* 2017; Chia *et al.* 2017; Cheng *et al.* 2018). Among the meiotically expressed LUTIs, 72 were found to be controlled by Ume6 based on ChIP-seq (Tresenrider *et al.* 2021). However, a more direct interrogation of Ume6's role in regulating these LUTIs remains unclear. Using the *UME6-AID* depletion system, we asked whether the Ume6-regulated LUTIs became derepressed in response to acute loss of *UME6* function during mitotic growth. Reads were aligned to a reference genome using HISAT2 and LUTI expression was monitored for all Ume6 regulated LUTIs. Of the 72 LUTIs, we identified 39 (54.2%) as being mitotically derepressed after Ume6 degradation (Supplementary Table 2). The remaining 35 failed to produce a detectable signal, possibly due to low expression and/or reduced transcript stability. Thus, our depletion system has validated a functional role for Ume6 in repressing at least 39 meiotically expressed LUTIs during mitotic growth, indicating that its activity as a transcriptional repressor can lead to both decreased and increased protein levels.

Diametric regulation of *UME6* expression by the meiotic transcription factors Ime1 and Ndt80

The 2 models for Ume6-dependent control of EMG expression were postulated based on different conclusions about the levels and timing of Ume6 degradation during meiosis. These differences may have stemmed from the asynchronous nature of meiotic entry and/or the use of *UME6* null allele, which causes significant growth defects during mitotic growth due to EMG derepression (Strich *et al.* 1994; Nachman *et al.* 2007). To investigate the role of *UME6* in the expression of EMGs, we first followed Ume6 protein levels in a population of cells undergoing highly synchronized meiotic progression. Synchronization of meiotic progression was achieved by using an established method that utilizes a copper-inducible promoter (*pCUP1*) to control the expression of 2 key regulators of meiotic entry: *IME1*, which encodes an early meiotic transcription factor, and *IME4*, which encodes an mRNA N6-adenosine methyltransferase (Berchowitz *et al.* 2013; Chia and van Werven 2016). We then monitored the abundance of an endogenously 3V5 tagged allele of *UME6* in these cells. Under the uninduced condition, Ume6 protein levels remained largely unchanged (Fig. 3a and b, uninduced). In contrast, induction of *IME1* and *IME4* (t = 2 h) resulted in a substantial increase in Ume6 protein levels, up to 8-fold, which was already evident 1 h following *pCUP1* induction (t = 3 h) and remained elevated until 7 h postinduction (Fig. 3a and b, *IME1*/4 induced). Thus, Ume6 protein levels actually increase following *IME1*/4 induction and remain elevated until around 7 h when cells transition out of prophase I.

To test whether Ume6 remained bound to EMG promoters following *IME1*/4 induction, we performed ChIP followed by quantitative PCR (ChIP-qPCR). Ume6 enrichment was monitored at the promoters of 3 well-characterized EMGs, *IME2*, *SPO13*, and *ZIP1*, as well as the ORF of *IME2* where Ume6 is not expected to bind. In the 3 EMGs analyzed, Ume6 remained bound at these promoters at levels similar to premeiotic conditions, irrespective of *IME1*/*IME4* induction. Thus, Ume6 is not displaced from EMG promoters during meiotic entry, suggesting that it plays a role in EMG activation during meiosis (Fig. 3c).

Given that *IME1* and *IME4* are involved in transcriptional and posttranscriptional gene regulation, respectively (Shah and Clancy 1992; Hongay *et al.* 2006; reviewed in van Werven and Amon 2011), we reasoned that the elevated Ume6 protein levels in meiosis could be due to an increase in *UME6* mRNA abundance and hence Ume6 synthesis. To investigate this further, we analyzed *UME6* transcripts by reverse transcription-quantitative PCR (RT-qPCR). In the absence of *IME1*/4 induction, *UME6* transcript levels were largely unchanged (Fig. 3d, *IME1*/4 uninduced). However, in response to *IME1*/4 induction, we observed ~7-fold increase in *UME6* transcript levels going from pre- to post-induction. This coincided with increased expression of the EMG *IME2* (Supplementary Fig. 2a). Furthermore, *UME6* transcript levels peaked after 5 h and remained high until 8 h, consistent with the immunoblotting data (Fig. 3a and d). Together, these findings demonstrate that *IME1*/4 induces the expression of both EMG and *UME6* and leads to elevated Ume6 protein levels during meiotic entry.

Following an initial increase, Ume6 protein levels began to decline after ~7 h in SPM. This timing coincided with the expression of *NDT80* (Fig. 3e), which encodes a transcription factor necessary for exit from meiotic prophase I, initiation of meiotic divisions, and gamete maturation (Xu *et al.* 1995). To directly test how Ndt80 influences Ume6, we took advantage of an inducible *NDT80* system whereby *NDT80* mRNA expression is triggered by a β-estradiol-activatable transcription factor (Benjamin *et al.* 2003; Carlile and Amon 2008). Cells were incubated in SPM for 5 h to achieve prophase I arrest, and then β-estradiol was withheld or added to the media, thereby either preventing or allowing for *NDT80* expression and progression through the meiotic divisions, respectively. In the absence of *NDT80* induction, Ume6 protein levels remained unchanged (Fig. 3f and g, uninduced). However, after 1.5 h following *NDT80* induction, Ume6 abundance was reduced to 32% of the initial levels and reached 15% after 4 h

(Fig. 3f and g, *NDT80* induced). To assess whether *NDT80* induction also influenced *UME6* transcript levels, RNA samples were collected for RT-qPCR. Withholding *NDT80* induction resulted in *UME6* transcript levels remaining largely unchanged (Fig. 3h; uninduced). In contrast, *NDT80* induction led to a ~32% drop in *UME6* transcript levels as early as 1.5 h (Fig. 3h; *NDT80* induced). We conclude that Ume6 protein levels decrease in response to Ndt80, not Ime1, and this downregulation is due in part to a reduction in *UME6* transcript levels. Downregulation of *UME6* following *NDT80* expression thus restricts the timing of Ume6 removal to when meiotic cells are transitioning from early to mid-meiotic gene expression.

Cdc20, which serves as an activator for the APC E3 ligase, has been previously implicated in Ume6 degradation based on the use of a temperature-sensitive *CDC20* allele (Mallory *et al.* 2007). Exposing cells to high temperatures is known to disrupt meiotic progression in a variety of organisms. Thus, the use a *cdc20-ts* allele may have confounding effects beyond *CDC20* inactivation. To circumvent this limitation, we utilized a meiotic-null allele of *CDC20*, *cdc20-mn*, and combined it with the inducible *NDT80* system (*pGAL-NDT80; GAL4-ER; pCLB2-CDC20*). However, Ume6 protein levels still declined in the *cdc20-mn* mutant following *NDT80* induction (Supplementary Fig. 2b and c). This finding is consistent with a previous report, which also found no evidence of Cdc20 involvement in Ume6 turnover during meiosis (Raithatha *et al.* 2021).

Our data thus far help differentiate Ume6's meiotic role in EMG activation through 3 key insights: (1) *IME1* expression results in the upregulation of *UME6* itself, leading to increased Ume6 protein levels; (2) Ume6 remains bound to the EMG promoters in the presence of Ime1; and (3) *NDT80* expression triggers events that lead to the downregulation of *UME6*, and thus reduced Ume6 protein levels, following exit from prophase I. These results are consistent with a model whereby Ime1 and Ume6 form an activator complex and once the early meiotic events are completed, *UME6* is downregulated in an Ndt80-dependent manner.

Meiotic depletion of Ume6 inhibits gamete formation and prevents proper activation of EMGs

Our findings support the notion that the Ime1-Ume6 activator complex drives the expression of EMGs; however, it remains unclear how loss of *UME6* function, specifically during gametogenesis, impacts meiotic progression and gene expression. To address this question, we combined *UME6-AID* with the inducible *IME1*/4 system, thus allowing us to rapidly deplete Ume6 shortly before meiotic entry. Our data thus far indicate that the Ume6 regulon contains at least 144 direct targets and that Ume6 is highly expressed during early meiosis, remaining bound to the EMG promoters. Thus, we predicted that depletion of Ume6 during meiosis would lead to a failure in EMG expression, disrupting gamete formation. To test the consequences of Ume6 depletion on meiosis, cells were cultured as before using the inducible *IME1*/4 system and were allowed to acclimate to SPM for 30 min. Ume6 depletion took place over the next 1.5 h at which point *IME1*/4 *was* induced. Samples for protein and RNA were collected prior to and following Ume6 depletion and *IME1*/4 induction. Consistent with our previous observations, in control cells, Ume6 protein levels increased by 58% as early as 30 min following *IME1*/4 induction and doubled by 4.5 h (Fig. 4a and b). In contrast, cells that were depleted for Ume6 experienced a noticeable drop in Ume6 protein levels, down to 30.6% of starting levels at 6 h (Fig. 4a and b; Supplementary Fig. 3a, please refer to *Materials and methods* for a detailed description of the differences between mitotic and meiotic depletion strains and conditions).

To determine the impact of Ume6 depletion on meiosis, we next analyzed the cells' ability to produce gametes, known as spores in yeast. For comparison, a strain containing only the inducible *IME1*/4 system (*pCUP1-IME1; pCUP1-IME4; UME6*) as well as an *IME1* null mutant (*ime1Δ*) where meiosis cannot occur was included (Fig. 4c). *ume6Δ* cells were too sick to process for the meiotic experiments. Sporulation efficiency was 95.3% for the *pCUP1-IME1*/4 strain and 0% for the *ime1Δ* mutant (Fig. 4c). In the control strain where Ume6 was not depleted, sporulation efficiency was 84%, indicating that our system experiences only minor deficiencies (Fig. 4c). In contrast, the Ume6 depletion strain displayed a severe reduction in sporulation efficiency (10%; Fig. 4c), indicating that acute removal of Ume6 inhibits cells' ability to complete the meiotic program.

To monitor how Ume6 depletion impacts the transcript levels of EMGs, we performed RNA-seq and analyzed our previously generated list of 144 mitotically repressed Ume6 targets to assess whether Ume6 was necessary for their meiotic expression. We monitored the Log2FC of average transcripts per million (TPM), which represent reads normalized to gene length, relative to the 2 h time point just before *IME1*/4 induction and found that the majority (112/144; 78%) of the mitotically repressed Ume6 targets now showed reduced expression upon Ume6 depletion relative to the control sample (Fig. 4d–f; Supplementary Fig. 3b–e).

To better highlight the genes that are most impacted by Ume6 depletion, we applied k-means clustering, which groups genes by their Euclidian distance while minimizing variation. Using the "elbow method," we found k = 3 to be optimal for subdividing our 144 genes in the Ume6 regulon (Thorndike 1953; Fritz *et al.* 2020). Group 1 contained 40 genes that were important for meiotic recombination and chromosome pairing, while group 2 had a combination of 72 meiotic and metabolic genes. Inspecting these subgroups, we found that genes in group 1 and 2 showed an average of ~43% and ~20% decrease in expression, respectively, in response to Ume6 depletion (Fig. 4d and e, comparing TPM for Ume6 depletion and control at 2.5 h). Indeed, Spearman analysis at 2.5 h for group 1 and 2 showed high dissimilarity between control and Ume6 depletion ($\rho = 0.435$ and 0.454, respectively; Supplementary Fig. 3c and d). This reduced expression and dissimilarity between conditions persisted until 6 h. Conversely, group 3 contained several different genes involved in meiosis, metabolism, and cell wall maintenance. Expression profiles for group 3 were overall more similar between control and Ume6 depletion (~3% increase in expression of the Ume6 depletion sample compared to control at 2.5 h). Consistently, Spearman analysis showed increased sample relatedness from 2.5 h until 6 h ($\rho =$ 0.74, 0.71, 0.86, and 0.88, at 2.5, 3, 4.5, and 6 h respectively; Fig. 4f and Supplementary Fig. 3e). Thus, depletion of Ume6 prior to *IME1*/4 induction disrupted 112 of our 144 Ume6 targets (78%), highlighting Ume6's importance in EMG activation during meiosis.

Focusing on 4 representative EMGs from group 1, *IME2*, *MEI5*, *SPO22*, and *RED1*, we found that differences in transcript levels were already detectable early on, since strains retaining a functional Ume6 (control) had lower basal expression levels, consistent with Ume6 acting repressively prior to *IME1* expression (Fig. 4d and g). Furthermore, in the control strain, gene expression spiked going from pre-*IME1*/4 induction at 2 h to post-*IME1*/4 induction at 2.5 h reaching 7-, 11-, 5-, and 4-fold, for *IME2*, *MEI5*, *SPO22*, and *RED1*, respectively (Fig. 4g). However, depletion of

Ume6 resulted in largely unchanged expression for *IME2*, *MEI5*, *SPO22*, and *RED1* (Fig. 4g, Ume6 Depletion). Taken together, the failure to form gametes combined with reduced transcript levels of meiotic genes in response to Ume6 depletion emphasizes the critical involvement of Ume6 in the expression of EMGs.

These findings demonstrate Ume6's dual role both as a repressor and an activator. By acutely depleting Ume6 under distinct developmental programs, we arrived at 2 very different outcomes. Mitotic depletion of Ume6 resulted in the derepression of its target genes, illustrating Ume6's role in ensuring EMG quiescence during the mitotic gene expression program (Fig. 4h). Consistently, depletion of Ume6 under nutrient-deprived conditions (i.e. in the absence of *IME1*) also led to derepression of EMGs (Fig. 4i; premeiotic). However, this level of EMG derepression was not sufficient to initiate meiosis. On the other hand, depletion of Ume6 shortly before *IME1/4* induction prevented the proper activation of EMGs, thereby exemplifying Ume6's second role as an activator of EMGs during the meiotic program (Fig. 4i). Thus, Ume6 serves as a primary determinant as to whether cells silence or induce the meiotic gene expression program depending on the cellular state and the associated cofactors.

Tethering of Ume6^{T99N} to Ime1 using the GFP nanobody trap system rescues meiotic defects associated with *UME6*^{T99N}

Previous studies have demonstrated that the meiotic kinase Rim11 phosphorylates both Ime1 and Ume6 to promote their interaction (Mitchell and Bowdish 1992; Rubin-Bejerano *et al.* 1996; Malathi *et al.* 1997). One key phosphorylation residue in Ume6 is Threonine 99 (T99). Indeed, a particular mutation at this position, T99N (Ume6^{T99N}), was found to severely reduce Rim11's ability to phosphorylate Ume6 (Bowdish *et al.* 1995; Malathi *et al.* 1997), thereby preventing binding of Ume6 to Ime1. To restore the interaction between Ime1 and Ume6^{T99N}, we utilized a GFP nanobody trap approach where Ume6^{T99N} carrying a 3V5 epitope was fused to the VH16 anti-GFP nanobody (*UME6*^{T99N}-3V5-*αGFP*; Fig. 5a; Fridy *et al.* 2014). For controls, we included *UME6*, *UME6*-3V5, and *UME6*^{T99N}-3V5. We then combined the *UME6* alleles with either *IME1* or an N-terminally GFP-tagged *IME1* at the endogenous locus (*GFP-IME1*; Moretto *et al.* 2018). If the interaction between Ime1 and Ume6 is sufficient to drive EMG expression, then in the *UME6*^{T99N}-3V5-*αGFP GFP-IME1* strain, where tethering occurs, sporulation should be rescued.

We first examined sporulation efficiency in the strains possessing different allelic combinations of *IME1* and *UME6*. For untagged *UME6*, the sporulation efficiency was >90% when combined with either untagged or GFP-tagged *IME1* (94.3 and 97.0%, respectively; Supplementary Fig. 4a). *UME6*-3V5 had a small drop in sporulation efficiency (92.7 and 89% for *IME1* and *GFP-IME1*, respectively; Fig. 5b), suggesting the tag mildly impairs *UME6* function. However, strains with *UME6*^{T99N}-3V5 had a severe defect in sporulation efficiency (27 and 18.7% for *IME1* and *GFP-IME1*, respectively). Addition of the GFP Nanobody to *UME6*^{T99N}-3V5 (*UME6*^{T99N}-3V5-*αGFP*) in cells containing untagged *IME1* further reduced the cell's sporulation efficiency to 9.0%. Despite this substantial drop in sporulation efficiency, when *UME6*^{T99N}-3V5-*αGFP* was paired with *GFP-IME1*, the sporulation efficiency was dramatically improved to 93.7% (Fig. 5b). Thus, restoring the interaction between Ume6 and Ime1 is sufficient to complete the meiotic program and produce gametes.

To investigate the extent to which the nanobody-based tethering of Ume6^{T99N} to Ime1 rescues the meiotic program, we collected RNA samples for various allelic combinations of *UME6* and *IME1* relative to their introduction to SPM at 0, 2, 4, and 6 h, to monitor EMG transcript abundance. First, we inspected 263 genes that are associated with driving early meiotic events based on previous studies (Mao-Draayer *et al.* 1996; Pâques and Haber 1999; Williams *et al.* 2002; Brar *et al.* 2012; Tresenrider *et al.* 2021). Eighty-nine of these genes were present in the Ume6 direct target list (Supplementary Table 1). In *UME6*-3V5 carrying either untagged or GFP-tagged *IME1*, many of these genes were upregulated after transfer to SPM (Fig. 5c, compare 0 vs 2, 4, 6 h). Introduction of *UME6*^{T99N}-3V5 resulted in a moderate disruption of EMG expression (Supplementary Fig. 4b). Consistent with the sporulation data, *UME6*^{T99N}-3V5-*αGFP* had a more severe defect in EMG expression than *UME6*^{T99N}-3V5 (Supplementary Fig. 4b). However, tethering of Ume6^{T99N} to Ime1 restored EMG expression back to WT (Supplementary Fig. 4b). This rescue was further supported by PCA, where points associated with *GFP-IME1; UME6*-3V5 *or GFP-IME1; UME6*^{T99N}-*αGFP* separated from untagged *IME1; UME6*^{T99N}-*αGFP* along PC1 (Supplementary Fig. 4c).

To globally identify the functional classes of genes expressed by tethering of Ime1 to Ume6, we performed DESeq2. Comparing *IME1* to *GFP-IME1* in the *UME6*^{T99N}-3V5-*αGFP* background, we identified 316 DEGs (padj < 0.05; log2FC > 1.5; 2 h in SPM; Supplementary Fig. 4d). Of these 316 DEGs, 137 were present in the EMG list and 70 were present in the Ume6 direct target list. GO enrichment revealed a number of early meiotic terms such as homologous recombination and SC formation, indicating that the tethering strategy restored early meiotic functions (Fig. 5e). Additionally, inspecting tethering results for our mitotic Ume6 target list showed a similar rescue in expression (Supplementary Fig. 4e and f). Finally, key EMGs including *IME2*, *ZIP1*, and *SPO13* displayed a strong rescue in their expression when Ume6^{T99N} was tethered to Ime1 (Fig. 5d). We note that at 0 h, use of the GFP nanobody trap resulted in unusually high expression for many EMGs (Fig. 5c and d). This is likely due to the high affinity between GFP and the αGFP antibody, which can bypass posttranslational regulations that control Ime1-Ume6 interaction and nuclear localization, thereby resulting in earlier meiotic initiation. Regardless, these data further corroborate the significance of Ime1-Ume6 interaction in establishing the meiotic program.

We also checked the magnitude and timing of *NDT80* expression along with its targets (Fig. 5f and g). In the *UME6*-3V5 control strain, *NDT80* expression remained low from 0 to 4 h at which point *NDT80* expression increased ~6.5 fold (Fig. 5g; from t = 4 to 6 h). Conversely, *NDT80* transcripts were largely unchanged in strains with *UME6*^{T99N}-3V5 or *UME6*^{T99N}-3V5-*αGFP*. However, tethering of Ume6^{T99N} to Ime1 led to upregulation of *NDT80* (Fig. 5g, ~11.3-fold increase from t = 4 to 6 h in the *UME6*^{T99N}-3V5-*αGFP; GFP-IME1* strain). Expression of *NDT80* is indicative of chromosome segregation and gamete maturation and several genes have been identified as upregulated during these events (Winter 2012; Cheng *et al.* 2018). Many of the Ndt80 target genes responded to formation of the Ime1-Ume6 complex, or lack thereof (Fig. 5f and g). Indeed, cells possessing *UME6*^{T99N}-3V5 or *UME6*^{T99N}-3V5-*αGFP* failed to activate these genes or did so at a reduced level (Fig. 5f and Supplementary Fig. 4g). In contrast, tethering of Ume6^{T99N} to Ime1 resulted in the timely activation of Ndt80 targets (Fig. 5f and g). Altogether, these findings further emphasize the importance of Ime1-Ume6 interaction while also demonstrating that bringing Ime1 in proximity of Ume6 is sufficient to drive meiotic initiation and gamete production.

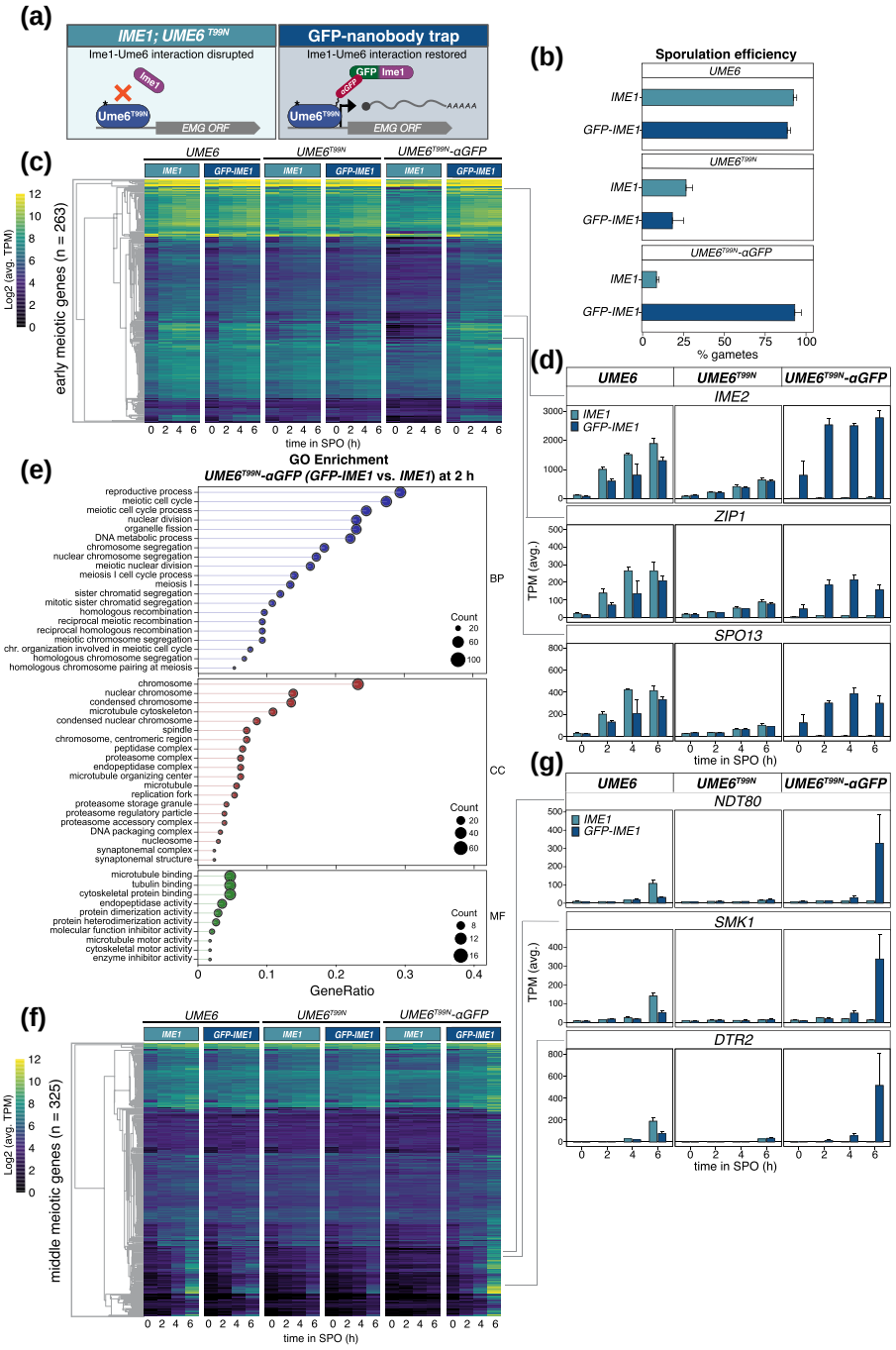

Fig. 5. Tethering of Ime1 and Ume6 using the GFP nanobody rescues the *UME6*^{T99N} meiotic defects. a) Illustration of the GFP-nanobody trap approach. The star on Ume6^{T99N} represents the T99N mutation within Ume6 that obstructs Ime1 from binding within this domain. b) Sporulation efficiency measured for strains containing either WT *IME1* and *UME6*-3V5 (UB26625), *UME6*^{T99N}-3V5 (UB26629), and *UME6*^{T99N}-3V5-*αGFP(VH16)* (UB27313), or *GFP-IME1* and *UME6*-3V5 (UB26641), *UME6*^{T99N}-3V5 (UB26645), and *UME6*^{T99N}-3V5-*αGFP(VH16)* (UB27243). 3V5 is not annotated in the figure labels for simplicity. Cells were grown in presporulation media before being transferred to SPM and allowed 24 h to complete the meiotic program before sporulation efficiency was measured. As before, 100 cells were counted and percentage of cells that formed tetrads was noted as % gametes for each allele combination and the average of 3 biological replicates is presented with the standard error. c–g) Strains used in (b) were transferred to SPM (t = 0 h), and RNA samples were collected at the designated times. RNA samples were processed as described in Fig. 3d, and TPM tables were generated from 3 biological replicates. To examine early gene response, a set of genes identified as early expressed by Williams *et al.* and Brar *et al.* and identified as *IME1* responsive by Tresenrider *et al.* were termed EMGs and monitored in our dataset. c) Heatmap representing Log2 of the mean TPM across 3 biological replicates for EMGs. Strains harboring distinct *UME6* alleles in combination with either untagged *IME1* or *GFP-IME1* are presented on top of the heatmap. d) Barplot representation for mean of TPM at a designated time point is shown for *IME2*, *ZIP1*, and *SPO13*. Standard error from 3 biological replicates is included. *UME6* alleles for each representative gene plot are shown at the top of their respective barplot. The gene represented by the barplot is shown at the top of each group and *IME1* allele is shown as either *IME1* or *GFP-IME1*. DESeq2 analysis between *IME1*; *UME6*^{T99N}-3V5-αGFP (UB27313), and *GFP-IME1*; *UME6*^{T99N}-3V5-αGFP (UB27243) at 2 h identified 316 DEGs (padj < 0.05). e) GO enrichment was used on the 316 DEGs that were upregulated (log2FC > 1.5). The gene ratio is shown on the x-axis and is the percent of genes in a given GO term out of the total 316 genes total. As before, the point size corresponds to the number of genes in that GO term while color signifies category: BP, biological process; CC, cellular component; MF, molecular function. f) Heatmap prepared as described in Fig. 5b representing a set of genes identified in Cheng *et al.* as responding to *NDT80* induction (Cheng *et al.* 2018). g) Barplots as prepared as described in (c) representing *NDT80*, *SMK1*, and *DTR2*.

Tethering of a heterologous AD to Ume6^{T99N} restores EMG expression, gamete formation, and viability

Since its initial discovery, Ime1 has been regarded as the master transcription factor in the activation of EMGs (Kassir *et al.* 1988). Strains lacking *IME1* (*ime1Δ*) fail to initiate meiosis and genetic screens have identified several mutations in *IME1* that disrupt meiotic initiation (Smith *et al.* 1993). Furthermore, mutations like *UME6*^{T99N} or depletion of Ume6, which block Ime1's ability to dock with Ume6 and localize to EMG promoters, also result in meiotic failure (this study; Mitchell and Bowdish 1992). Thus, Ime1 is an essential factor in launching the meiotic transcriptional program.

On the other hand, the modularity of transcription factors has long been appreciated (Hahn and Young 2011). In fact, Ime1 itself can be broken into 3 distinct subdomains: an AD, a nutrient-responsive domain, and a Ume6 interaction domain (Smith *et al.* 1993). Here, we found that tethering of Ime1 to Ume6^{T99N} is sufficient to initiate the meiotic program. We reasoned that this may occur because: (1) Ume6 needs to associate with an AD in order to function as a coactivator or (2) Ime1 has additional functions besides serving as a transactivator, which are restored upon recruitment to Ume6. To distinguish between these possibilities, we employed a heterologous AD from *E. coli*, known as B112 (Ottoz *et al.* 2014), and kept it either untagged or fused to GFP (Fig. 6a). As controls, we used Ime1 or GFP-Ime1 (Fig. 6a). Each transgene was integrated at the *HIS3* locus and was tested for its ability to suppress *ime1Δ* in the *UME6*^{T99N}-3V5-*αGFP* background. All constructs were placed under the control of the *IME1* promoter to maintain physiological regulation and transgene expression was confirmed by immunoblotting (Supplementary Fig. 5a). Meiotic initiation through tethering of a heterologous AD to Ume6 would suggest that Ume6 is the primary determinant of EMG activation through its association with a transactivator. Conversely, failure to initiate meiosis would indicate a unique role for Ime1 in conducting the meiotic program.

To test whether B112 could rescue the defects associated with *ime1Δ*, we first measured sporulation efficiency in the *UME6*^{T99N}-3V5-*αGFP* background. As expected, in strains carrying an untagged *B112* or *IME1* allele, no spores were formed (Supplementary Fig. 5b). *GFP-IME1* strain mostly produced tetrads (92%) and a few dyads (4%). Interestingly, *GFP-B112* also produced several tetrads (71.7%) and some dyads (10.3%) (Fig. 6b). We next examined gamete viability for the strains that underwent sporulation. We found that 92.6% of the gametes from *GFP-IME1* were viable (Fig. 6c and d). Notably, the *GFP-B112* strain also had high gamete viability of 93.2%, though colonies were marginally smaller (Fig. 6c and d). These results demonstrate that tethering of either Ime1 or a heterologous AD to Ume6 is sufficient to induce meiosis and generate viable gametes.

Next, we performed RNA-seq to gain insights into the underlying response from the transcriptome. First, we analyzed global differences between samples using Spearman's rank correlation. We find that differences between strains carrying untagged *IME1* or *B112* transgenes were minimal (Supplementary Fig. 5c). However, comparison between untagged and GFP-fused transgenes showed a stark difference (Supplementary Fig. 5c). Interestingly, comparison of *GFP-IME1* to *GFP-B112* revealed high correlation at earlier time points ($\rho = 0.960$ and 0.912 at 0 and 2 h, respectively), but divergence at later time points ($\rho = 0.757$ and 0.848 at 4 and 6 h, respectively). We observed similar patterns using PCA (Supplementary Fig. 5d). These results indicate that the gene expression profiles of *GFP-IME1* and *GFP-B112* start similarly but diverge from one another later in meiosis.

Next, we focused on the EMGs previously shown to respond to *IME1* induction (Tresenrider *et al.* 2021) and visualized them on a heatmap (Fig. 6e). *GFP-IME1* and *GFP-B112* resulted in higher EMG expression compared to their untagged counterparts. However, while EMG expression in *GFP-IME1* began to decrease at 4 and 6 h, EMGs remain elevated in *GFP-B112*. Looking more closely at *IME2*, *SPO13*, and *ZIP1*, we observed a pattern where these transcripts in *GFP-IME1* and *GFP-B112* were at their highest at 0 h (Fig. 6f). In the *GFP-IME1* strain, *IME2*, *SPO13*, and *ZIP1* transcript levels were reduced by nearly half every 2 h. Conversely, in the *GFP-B112* strain, *IME2*, *SPO13*, and *ZIP1* transcript levels increased subtly after 2 h in SPM (Fig. 6f). Furthermore, the Ume6 mitotic targets identified in this study were expressed in both *GFP-IME1* and *GFP-B112* (Supplementary Fig. 5e and f). To identify when peak expression of EMGs occurred in *GFP-IME1* and *GFP-B112*, we applied gene set enrichment analysis (GSEA; Mootha *et al.* 2003; Subramanian *et al.* 2005). GSEA revealed that EMG enrichment was highest at 2 h for *GFP-IME1* (Normalized Enrichment Score (NES) = 3.93; Fig. 6g). Conversely, in *GFP-B112*, EMGs were most enriched at 6 h (NES = 4.21). Thus, when both Ime1 and B112 are recruited to Ume6 through artificial tethering, cells are able to trigger EMG expression, albeit with different dynamics.

To understand the differences between *GFP-IME1* and *GFP-B112* at t = 6 h that may cause these discrepancies in EMG expression, we performed DESeq2. DESeq2 identified 543 DEGs enriched in *GFP-IME1* compared to *GFP-B112*, several of which were middle meiotic genes (MMGs) including *NDT80* (padj < 0.05; log2FC > 1.5; Supplementary Fig. 6a). Consistent with this, GO enrichment terms were largely involved in ascospore wall development, a process controlled by *NDT80* (Supplementary Fig. 6b). Thus, the prolonged expression of EMGs in *GFP-B112* may relate to a delay in meiotic progression. The downregulation of EMGs and exit from meiotic prophase is largely dependent on activation of *NDT80* and its targets (Xu *et al.* 1995; Brar *et al.* 2012; Okaz *et al.* 2012; Chia *et al.* 2021). To determine whether *GFP-B112* also delays *NDT80* expression, we monitored *NDT80* transcript levels in our dataset along with many of its downstream targets (Cheng *et al.* 2018). We first visualized *NDT80* and its targets by heatmap (Fig. 7a). During early time points (t = 0–2 h) *NDT80* expression was low in both *GFP-B112* and *GFP-IME1* along with 2 of its targets *SMK1* and *DTR2* (Fig. 7b). *NDT80* transcript level increased in *GFP-IME1* by ~5.7 fold going from 2 to 4 h, whereas *NDT80* levels in *GFP-B112* only began increasing going from 4 to 6 h (~4.5 fold). Similar results were observed for the Ndt80-targets *SMK1* and *DTR2*. To determine whether the delay in *NDT80* expression extended to *NDT80* targets in the *GFP-B112* strain, we analyzed these genes in our dataset (*NDT80* target list was obtained from Cheng *et al* 2018). Using GSEA, we observed that the highest enrichment of *NDT80* targets occurred around 4 and 6 h for *GFP-IME1* (NES = 3.74 and 3.75, respectively; Fig. 7c). Conversely, enrichment of *NDT80* targets in *GFP-B112* did not occur until 6 h (NES = 3.16) and was not as strong compared to *GFP-IME1* (Fig. 7c). Taken together, our results indicate that *GFP-IME1* and *GFP-B112* are able to initiate the meiotic program and produce viable gametes in the *UME6*^{T99N}-3V5-*αGFP* background. However, while *GFP-IME1* appears to achieve this in a timely manner, *GFP-B112* appears to have an extended meiotic prophase and subsequent delay in *NDT80* expression.

To further confirm a delay in meiotic progression, we used an endogenously fluorescent tagged histone H2B (*HTB1-mCherry*)

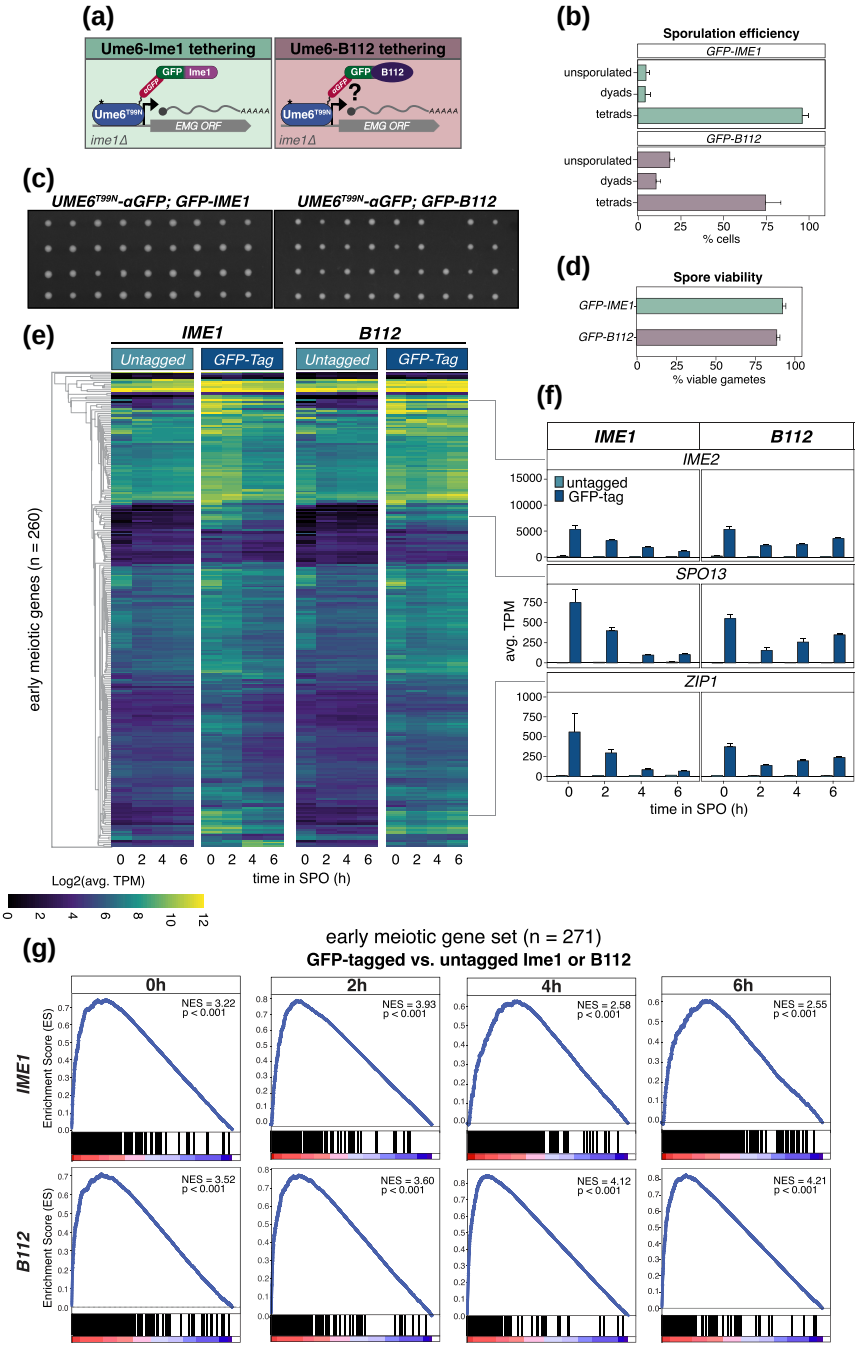

Fig. 6. Artificial tethering of the heterologous B112 AD to Ume6^{T99N} is sufficient to induce meiosis and produce viable gametes. a) Illustration of the GFP-Nanobody trap approach using *IME1* and the heterologous AD *B112* to suppress *ime1Δ* in a *UME6*^{T99N}*-3V5-αGFP(VH16)*. The star present on Ume6^{T99N} represents the point mutation T99N that prevents Ime1 from associating normally with Ume6 within this region. Sporulation efficiency was measured for strains harboring *ime1Δ* and *UME6*^{T99N}*-3V5-αGFP(VH16)* with either untagged *IME1* (UB32574), *GFP-IME1* (UB32572), untagged *B112* (UB33048), or *GFP-B112* (UB30295). One hundred cells were counted to determine the percentage of unsporulated cells, dyads or tetrads. Data from 3 biological replicates along with standard error are displayed. c) Strains harboring both *ime1Δ* and *UME6*T99N-3V5-*αGFP(VH16)* with *GFP-IME1* (UB32572) or *GFP-B112* (UB30295) were transferred to SPM and allowed to complete the meiotic program for 48 h. Spore viability was tested by digesting tetrads in zymolase 100 T (1 mg/mL) for 12 min before dissecting them onto nutrient rich YPD agar plates. Representative plates from the dissections are shown for *GFP-IME1*(UB32572) and *GFP-B112* (UB30295). d) Quantification of spore viability. Spore viability was defined as the percent of spores that formed colonies after being transferred to nutrient rich plates out of the total 296. Note that untagged ADs failed to produce spores and were therefore not included in the analysis. e and f) Strains containing both *ime1Δ* and *UME6*^{T99N}*-3V5-αGFP(VH16)* with either untagged *IME1* (UB32574), *GFP-IME1* (UB32572), untagged *B112* (UB33048), or *GFP-B112* (UB30295) were transferred to SPM (t = 0 h) and RNA samples were collected at the specified times. Heatmaps for EMGs were generated as described previously and represent log2 of the mean for 3 biological replicates. *UME6*^{T99N}*-3V5-αGFP(VH16)* is present in combination with *IME1* (left) or *B112* (right) either untagged or GFP-tagged in both heatmaps. f) Barplot showing mean TPM for the indicated genes for either untagged or GFP-tagged *IME1* (left column) or *B112* (right column). g) Gene set enrichment analysis (GSEA) comparing untagged and sfGFP-tagged *IME1* (top) or *B112* (bottom) for "EMGs" at designated time points. The curved line represents enrichment for a set of genes in a given sample and the peak position denotes the degree to which that set is over- or underrepresented. The enrichment score was then normalized to account for gene set variation and is presented as normalized enrichment score (NES). Vertical bars represent a gene and its position along the heatmap (bottom) shows how enriched that gene is in either *GFP-AD* (left-side) or untagged *AD* (right-side).

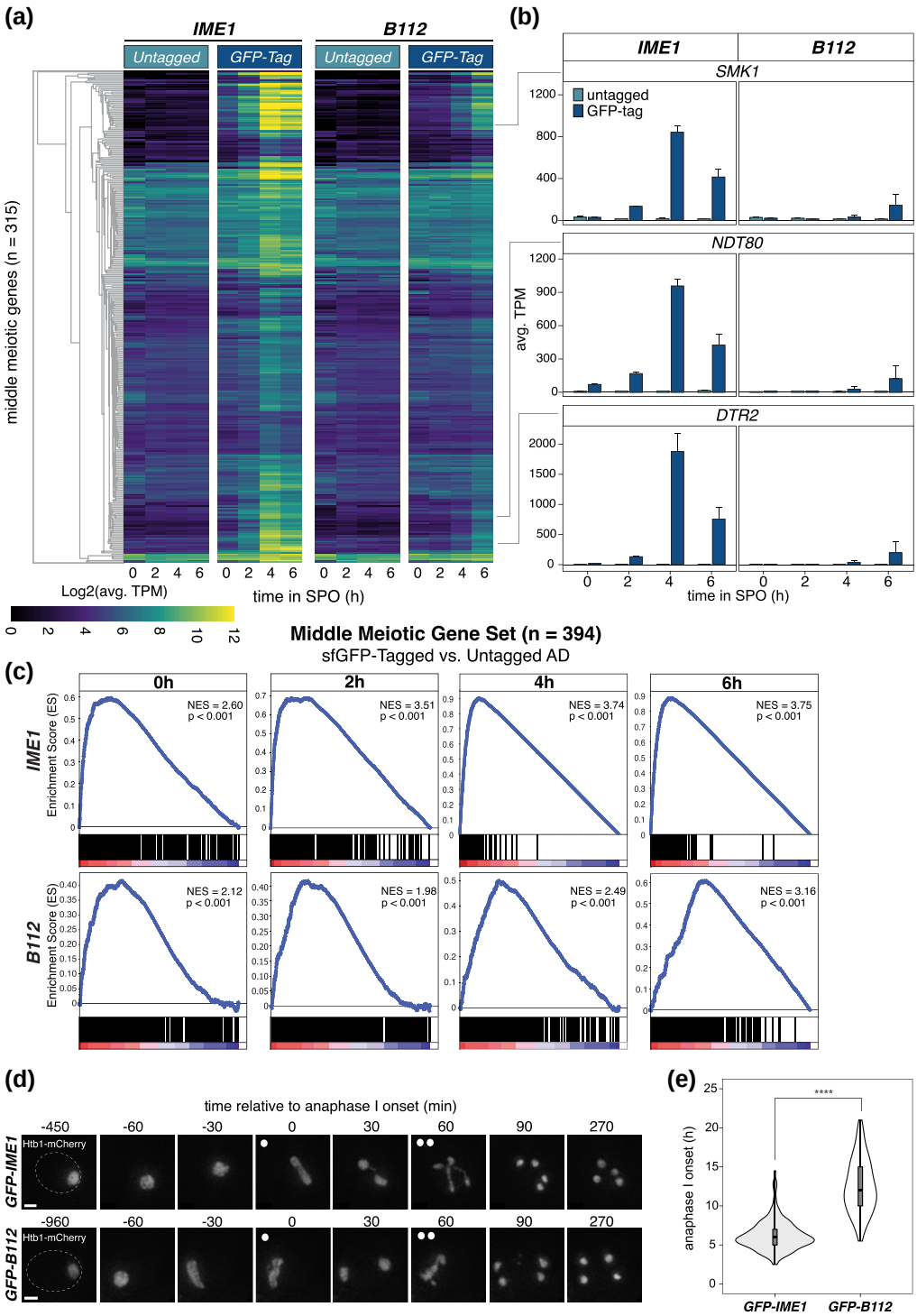

Fig. 7. Middle meiotic gene expression is delayed with the B112 AD. a and b) Cells were prepared as in Fig. 6. Heatmaps for middle meiotic genes (A) and (B) were made as previously described and represent log2 of the mean for 3 biological replicates. *UME6*^{T99N}-3V5-*αGFP(VH16)* was combined with either *IME1* (left) or *B112* (right) lacking or possessing the GFP-tagged, respectively. b) Barplot showing mean TPM for the indicated genes for either untagged or GFP-tagged *IME1* (left column) or *B112* (right column). c) GSEA was applied as in Fig. 6e. This time using the NDT80 cluster from Cheng *et al.* (2018) to observe enrichment of *NDT80* and its downstream targets, here called "middle meiotic genes." d and e) Cells were transferred to SPM after brief sonication and using the CellASIC Platform in an environmentally controlled chamber at 30 °C, pictures were acquired at 30 min intervals for over 21 h. d) Representative images for Z-projected cells carrying either *GFP-IME1* (UB32625) or *GFP-B112* (UB31729) at the specified times. Using HTB1-mCherry, a histone marker, we labeled chromatin to identify anaphase I onset. Anaphase I is defined as the start of chromatin bifurcating into 2 distinct foci. Onset of anaphases I and II are denoted by either 1 or 2 circles. Scale bar, 2 μm. Dashed lines represent cell boundary. e) Quantification of anaphase I onset in cells containing *GFP-IME1* or *GFP-B112* are presented as a violin plot containing a box plot. For *GFP-IME1*, 191 cells were counted and average time to anaphase I onset was 6.2 h. For *GFP-B112*, 162 cells were counted and average time to anaphase I onset was 12.5 h. *t*-test results are presented on the graph and show differences in the population $t(352) = -21.8$, $P < 0.00001$ (****) in a 1-tailed test.

and performed time-lapse microscopy. We observed a delay in the onset of anaphase I in the *GFP-B112* strain (Fig. 7d and e). While *GFP-IME1* cells took ~6.2 h ($n = 191$, SD = 1.9 h) to initiate anaphase I, *GFP-B112* cells took 12.5 h ($n = 162$, SD = 3.4 h) to reach anaphase I ($P < 0.00001$; 1-tailed *t*-test). We find that this slowdown of meiotic progression is consistent with the delayed activation of the *NDT80* regulon in *GFP-B112*. However, despite the delay in *GFP-B112* cells, once initiated the divisions are completed with similar timing compared to *GFP-IME1* (Fig. 7d).

Taken altogether, these data support a model where Ime1's association with Ume6 generates an activator complex to induce EMGs. Removal or disruption of the interaction between Ime1 and Ume6 hinders meiotic entry. Furthermore, EMGs can be activated when a heterologous AD is tethered to Ume6 indicating that generic transcriptional activators are able to initiate the meiotic program and even produce viable gametes when targeted to the correct genomic locations. This suggests that Ime1 serves chiefly as transactivator for Ume6 and that Ime1 has been evolutionarily tuned to allow timely expression of EMGs and execution of the meiotic program.

Discussion

Our study demonstrates that the transcription factor Ume6 is essential for gametogenesis. Importantly, we show that the meiotic regulator Ime1 primarily functions as a transactivator within the Ume6-Ime1 complex since a heterologous AD from bacteria can largely substitute for Ime1. These findings place Ume6 at the center of EMG regulation and demonstrate its essentiality in the proper execution of the meiotic transcriptional program.

Ume6 controls its own expression through a URS1 motif

Ume6 protein levels remain constant in the absence of *IME1* expression. However, induction of *IME1* and *IME4* leads to a dramatic increase in *UME6* transcript levels, resulting in an upsurge in Ume6 protein abundance (Fig. 3a and b). These findings indicate that Ume6 is not degraded in response to *IME1* expression, as previously postulated (Mallory *et al.* 2007; Mallory *et al.* 2012; Law *et al.* 2014), but is rather upregulated. Consistently, published datasets (Chia *et al.* 2021; Tresenrider *et al.* 2021) indicate a URS1 site proximal to the *UME6* transcriptional start site (TSS). The URS1 is located −147 bp upstream of the *UME6* TSS, suggesting that Ume6 is regulating its own promoter. We further observed meiotic upregulation of *UME6* through tethering of Ume6 to a heterologous AD (Supplementary Fig. 5f). Taken altogether, Ume6 appears to stimulate its own expression during meiotic entry through a URS1 motif. Interestingly, *IME1* is also known to regulate its promoter through a URS1 motif (van Werven *et al.* 2012; Moretto *et al.* 2021). This indicates that cells have evolved feed-forward mechanisms that ensure both Ime1 and Ume6 are present at sufficient levels during meiotic entry. In addition to the feed-forward regulation by Ime1-Ume6, *IME1* mRNA is further stabilized by Ime4, which functions as an N6-adenosine methyltransferase (Shah and Clancy 1992; Hongay *et al.* 2006). However, it is currently unknown whether *UME6* mRNA is also regulated by Ime4. Future work could reveal more commonality between transcriptional and posttranscriptional control of *IME1* and *UME6*.

If Ume6 regulates its own promoter, then formation of the Ume6-Sin3-Rpd3 complex in mitotic cells would be expected to repress *UME6* expression during vegetative growth. Ume6 is expressed during vegetative growth, albeit at low levels (Fig. 2d). Furthermore, mitotic depletion of Ume6 leads to a modest upregulation of *UME6* transcripts (Fig. 2d). Thus, Ume6 appears to repress its own transcription during mitotic growth but to a much lesser extent than the EMGs, which are essentially quiescent in mitotically dividing cells. It has been shown that in addition to Sin3-Rpd3, Ume6 also associates with the chromatin remodeler Isw2 for full repression of EMGs (Goldmark *et al.* 2000; Donovan *et al.* 2021). Whether Ume6, Sin3-Rpd3, and Isw2 work together at the *UME6* promoter and how they simultaneously achieve silencing of the EMGs requires further investigation.

UME6-AID system refines the Ume6 regulon

Of the 144 Ume6 direct targets identified in this study, 86.1% (124/144) were also present in the *ume6Δ* mutant (Supplementary Fig. 1g). *ume6Δ* has 1,143 additional DEGs with a padj < 0.05 and log2FC > 0.6 (Supplementary Table 3). This large number of DEGs is likely due to the severe growth defect associated with *ume6Δ* and hence represents a combination of direct and indirect effects. Thus, the AID system helped to circumvent many of the pleiotropic or secondary effects associated with the *ume6Δ* mutants, while also contributing heavily to our understanding of the Ume6 regulon.

Ume6 and Ime1 form an activator complex to drive EMG expression during gametogenesis

Our findings indicate that Ume6 and Ime1 form an activator complex to drive EMG expression. Besides upregulation of *UME6* following meiotic entry, 4 lines of evidence are consistent with this interpretation: First, depletion of Ume6 shortly before *IME1* activation disrupts EMG expression and gamete formation (Fig. 4). Second, Ume6's association with EMG promoters is unaffected by *IME1* expression (Fig. 3c). Third, rescuing the interaction between $Ume6^{T99N}$ and Ime1 using a nanobody trap approach leads to an increase in Ume6 levels, rather than promoting its degradation, and enables activation of EMGs as well as meiotic execution (Fig. 5). Finally, substitution of Ime1 with a heterologous AD from bacteria is sufficient to induce EMG expression and production of viable gametes in a Ume6-dependent manner, albeit the kinetics of this were reduced (Fig. 6). This finding also suggests that Ime1 is unlikely to possess an additional function beyond serving as a finely tuned transactivator for Ume6.

The transcription factor Ndt80 downregulates Ume6 following exit from meiotic prophase

Ume6 protein levels decrease during mid, rather than early, meiosis in response to *NDT80* expression. Ndt80's involvement in *UME6* downregulation comes at a time when many early meiotic events must be terminated. Although Ime1 remains bound to Ume6 during meiosis, it has been shown that Ime1 is unable to fully initiate EMG expression mitotically while Sin3-Rpd3 is bound to Ume6 (Smith *et al.* 1990). Thus, Ndt80 could influence Sin3-Rpd3 in the downregulation of both EMGs and *UME6*. Whether Rpd3 is bound to EMG promoters during meiosis is ambiguous. Some studies suggest that Rpd3 is enriched at the *IME2* promoter during meiosis (Inai *et al.* 2007; Raithatha *et al.* 2021) while others have found Rpd3 signal to be transiently lost (Pnueli *et al.* 2004). It is unclear where the discrepancy arises and has left Sin3-Rpd3's involvement largely unresolved. However, the list of genes responsive to Ndt80 activation is quite expansive (Cheng *et al.* 2018). A target of Ndt80 may function to reduce or reverse the effects of Ume6 phosphorylation by Rim11 and/or Rim15 permitting Sin3-Rpd3 to reestablish a repressive state for EMGs. Further investigation is required to understand the mechanism by which Ndt80 mediates *UME6* downregulation and the biological significance of such regulation.

Concluding remarks

Our findings implicate Ume6 as a major determinant of EMG expression and successful meiotic execution. Through binding to a transcriptional activator, like Ime1, Ume6 is converted from a repressor to an activator. As part of the Ime1-Ume6 coactivator complex, both *IME1* and *UME6* appear to engage in a feed-forward mechanism by harboring a URS1-motif in their promoters. This mechanism ensures adequate protein levels and proper EMG expression through promoting their own mRNA production. Removal of Ume6 prior to *IME1* and *IME4* induction is deleterious for meiotic success and EMG expression. Furthermore, mutants that prevent proper Ime1 and Ume6 interaction also disrupt meiotic initiation. However, through reuniting Ume6 with even a heterologous AD, EMG expression and the meiotic program can be rescued.

This reliance on formation of an activator complex is functionally analogous to mammalian systems, where MEIOSIN and STRA8 form a complex to drive meiotic initiation. MEIOSIN, like Ume6, has been shown to bind to promoters of EMGs and recruit STRA8 to those sites (Ishiguro *et al.* 2020). Additionally, like Ime1, STRA8 has been shown to carry the AD necessary for EMG activation (Tedesco *et al.* 2009; Ishiguro *et al.* 2020). *Meiosin* KO strains fail to initiate meiosis even in the presence of STRA8 (Ishiguro *et al.* 2020). The functional similarities between STRA8-MEIOSIN and Ime1-Ume6 are striking. Therefore, our study could shed light into the transcriptional regulation of meiotic entry in more complex systems and provide a lens to investigate the associated meiotic defects.

Data availability

All reagents used in this study are available upon request from the corresponding author. Sequencing data generated in this study are available are available at NCBI GEO under the accession ID: GSM7083402 through GSM7083623. The custom code used for the analysis is available in the following code repository: https://github.com/harranth.

Supplemental material available at GENETICS online.

Acknowledgments

We thank Gloria Brar, Doug Koshland, Peter Sudmant, Kathleen Ryan, Folkert van Werven, Andrea Higdon, Amanda Su, Amy Tresenrider, Ben Styler, Cyrus Ruediger, Emily Powers, Grant King, Jingxun Chen, Jessica Leslie, Kate Morse, and Tina Sing for suggestions and comments on this manuscript, Amy Tresenrider, Peter Sudmant, Christopher Mugler, Grant King, Jingxun Chen, Lizet Reyes, and Tina Sing for technical support, Jeremy Thorner, and all members of the Ünal and Brar labs for valuable discussions.

Funding

This work is supported by funds from the National Institutes of Health (R01 GM140005) and Astera Institute to E.Ü. A.H is supported by a Chancellor's Fellowship endowed by the University of California, Berkeley, and by funding from the National Science Foundation Graduate Research Fellowships Program (DGE-1752814).

Conflicts of interest

The authors declare no conflict of interest.

Author contributions

A.H.: conceptualization, data curation, formal analysis, investigation, methodology, validation, visualization, and drafting of the manuscript. E.Ü.: conceptualization, visualization, supervision, project administration, funding acquisition, and drafting of the manuscript.

Literature cited

Bailey TL, Elkan C. Fitting a mixture model by expectation maximization to discover motifs in biopolymers. Proc Int Conf Intell Syst Mol Biol. 1994;2:28–36.

Bailey TL, Johnson J, Grant CE, Noble WS. The MEME suite. Nucleic Acids Res. 2015;43(W1):W39–W49. doi:10.1093/nar/gkv416.

Balakrishnan R, Park J, Karra K, Hitz BC, Binkley G, Hong EL, Sullivan J, Micklem G, Michael Cherry J. Yeastmine—an integrated data warehouse for *Saccharomyces cerevisiae* data as a multipurpose tool-kit. Database. 2012;2012:bar062. doi:10.1093/database/bar062.

Benjamin KR, Zhang C, Shokat KM, Herskowitz I. Control of landmark events in meiosis by the CDK Cdc28 and the meiosis-specific kinase Ime2. Genes Dev. 2003;17(12):1524–1539. doi:10.1101/gad.1101503.

Berchowitz LE, Gajadhar AS, van Werven FJ, Rosa AAD, Samoylova ML, Brar GA, Xu Y, Xiao C, Futcher B, Weissman JS, *et al.* A developmentally regulated translational control pathway establishes the meiotic chromosome segregation pattern. Genes Dev. 2013;27(19):2147–2163. doi:10.1101/gad.224253.113.

Bowdish KS, Mitchell AP. Bipartite structure of an early meiotic upstream activation sequence from *Saccharomyces cerevisiae*. Mol Cell Biol. 1993;13(4):2172–2181. doi:10.1128/mcb.13.4.2172-2181.1993

Bowdish KS, Yuan HE, Mitchell AP. Positive control of yeast meiotic genes by the negative regulator UME6. Mol Cell Biol. 1995;15(6):2955–2961. doi:10.1128/MCB.15.6.2955.

Brar GA, Yassour M, Friedman N, Regev A, Ingolia NT, Weissman JS. High-resolution view of the yeast meiotic program revealed by ribosome profiling. Science. 2012;335(6068):552–557. doi:10.1126/science.1215110.

Bray NL, Pimentel H, Melsted P, Pachter L. Near-optimal probabilistic RNA-seq quantification. Nat Biotechnol. 2016;34(5):525–527. doi:10.1038/nbt.3519.

Carlile TM, Amon A. Meiosis I is established through division-specific translational control of a cyclin. Cell. 2008;133(2):280–291. doi:10.1016/j.cell.2008.02.032.

Carlson M. org.Sc.sgd.db: genome wide annotation for yeast; 2021. [accessed 2023 Feb]. https://yeastmine.yeastgenome.org/yeastmine/begin.do.

Chen J, Tresenrider A, Chia M, McSwiggen DT, Spedale G, Jorgensen V, Liao H, van Werven FJ, Ünal E. Kinetochore inactivation by expression of a repressive mRNA. Elife. 2017;6:e27417. doi:10.7554/eLife.27417.

Cheng Z, Otto GM, Powers EN, Keskin A, Mertins P, Carr SA, Jovanovic M, Brar GA. Pervasive, coordinated protein-level changes driven by transcript isoform switching during meiosis. Cell. 2018;172(5):910–923.e16. doi:10.1016/j.cell.2018.01.035.

Chia M, Li C, Marques S, Pelechano V, Luscombe NM, van Werven FJ. High-resolution analysis of cell-state transitions in yeast suggests widespread transcriptional tuning by alternative starts. Genome Biol. 2021;22(1):34. doi:10.1186/s13059-020-02245-3.

Chia M, Tresenrider A, Chen J, Spedale G, Jorgensen V, Ünal E, van Werven FJ. Transcription of a 5′ extended mRNA isoform

directs dynamic chromatin changes and interference of a downstream promoter. Elife. 2017;6:e27420. doi:10.7554/eLife.27420.

Chia M, van Werven FJ. Temporal expression of a master regulator drives synchronous sporulation in budding yeast. G3 (Bethesda). 2016;6(11):3553–3560. doi:10.1534/g3.116.034983.

Colomina N, Garí E, Gallego C, Herrero E, Aldea M. G1 cyclins block the Ime1 pathway to make mitosis and meiosis incompatible in budding yeast. EMBO J. 1999;18(2):320–329. doi:10.1093/emboj/18.2.320.

Colomina N, Liu Y, Aldea M, Garí E. TOR Regulates the subcellular localization of Ime1, a transcriptional activator of meiotic development in budding yeast. Mol Cell Biol. 2003;23(20):7415–7424. doi:10.1128/MCB.23.20.7415-7424.2003.

Donovan DA, Crandall JG, Truong VN, Vaaler AL, Bailey TB, Dinwiddie D, Banks OG, McKnight LE, McKnight JN. Basis of specificity for a conserved and promiscuous chromatin remodeling protein. Elife. 2021;10:e64061. doi:10.7554/eLife.64061.

Feichtinger J, McFarlane RJ. Meiotic gene activation in somatic and germ cell tumours. Andrology. 2019;7(4):415–427. doi:10.1111/andr.12628

Fridy PC, Li Y, Keegan S, Thompson MK, Nudelman I, Scheid JF, Oeffinger M, Nussenzweig MC, Fenyö D, Chait BT, *et al.* A robust pipeline for rapid production of versatile nanobody repertoires. Nat Methods. 2014;11(12):1253–1260. doi:10.1038/nmeth.3170.

Fritz M, Behringer M, Schwarz H. LOG-means: efficiently estimating the number of clusters in large datasets. Proc VLDB Endow. 2020;13(12):2118–2131. doi:10.14778/3407790.3407813.

Gibson DG, Young L, Chuang R-Y, Venter JC, Hutchison CA, Smith HO. Enzymatic assembly of DNA molecules up to several hundred kilobases. Nat Methods. 2009;6(5):343–345. doi:10.1038/nmeth.1318.

Goldmark JP, Fazzio TG, Estep PW, Church GM, Tsukiyama T. The Isw2 chromatin remodeling complex represses early meiotic genes upon recruitment by Ume6p. Cell. 2000;103(3):423–433. doi:10.1016/S0092-8674(00)00134-3.

Hahn S, Young ET. Transcriptional regulation in Saccharomyces cerevisiae: transcription factor regulation and function, mechanisms of initiation, and roles of activators and coactivators. Genetics. 2011;189(3):705–736. doi:10.1534/genetics.111.127019.

Hanahan D, Weinberg RA. Hallmarks of cancer: the next generation. Cell. 2011;144(5):646–674. doi:10.1016/j.cell.2011.02.013.

Hassold T, Hunt P. To err (meiotically) is human: the genesis of human aneuploidy. Nat Rev Genet. 2001;2(4):280–291. doi:10.1038/35066065.

Hongay CF, Grisafi PL, Galitski T, Fink GR. Antisense transcription controls cell fate in *Saccharomyces cerevisiae*. Cell. 2006;127(4):735–745. doi:10.1016/j.cell.2006.09.038.

Inai T, Yukawa M, Tsuchiya E. Interplay between chromatin and trans-acting factors on the IME2 promoter upon induction of the gene at the onset of meiosis. Mol Cell Biol. 2007;27(4):1254–1263. doi:10.1128/MCB.01661-06.

Ishiguro K, Matsuura K, Tani N, Takeda N, Usuki S, Yamane M, Sugimoto M, Fujimura S, Hosokawa M, Chuma S, *et al.* MEIOSIN directs the switch from mitosis to meiosis in mammalian germ cells. Dev Cell. 2020;52(4):429–445.e10. doi:10.1016/j.devcel.2020.01.010.

Janke C, Magiera MM, Rathfelder N, Taxis C, Reber S, Maekawa H, Moreno-Borchart A, Doenges G, Schwob E, Schiebel E, *et al.* A versatile toolbox for PCR-based tagging of yeast genes: new fluorescent proteins, more markers and promoter substitution cassettes. Yeast. 2004;21(11):947–962. doi:10.1002/yea.1142.

Kassir Y, Granot D, Simchen G. IME1, a positive regulator gene of meiosis in *S. cerevisiae*. Cell. 1988;52(6):853–862. doi:10.1016/0092-8674(88)90427-8.

King GA, Goodman JS, Schick JG, Chetlapalli K, Jorgens DM, McDonald KL, Ünal E. Meiotic cellular rejuvenation is coupled to nuclear remodeling in budding yeast. Elife. 2019;8:e47156. doi:10.7554/eLife.47156.

King GA, Wettstein R, Varberg JM, Chetlapalli K, Walsh ME, Gillet LCJ, Hernández-Armenta C, Beltrao P, Aebersold R, Jaspersen SL, *et al.* Meiotic nuclear pore complex remodeling provides key insights into nuclear basket organization. J Cell Biol. 2022;222(2):e202204039. doi:10.1083/jcb.202204039.

Law MJ, Mallory MJ, Dunbrack RL, Strich R. Acetylation of the transcriptional repressor Ume6p allows efficient promoter release and timely induction of the meiotic transient transcription program in yeast. Mol Cell Biol. 2014;34(4):631–642. doi:10.1128/MCB.00256-13.

Li K. The image stabilizer plugin for ImageJ; 2008. [accessed 2022 Sep 22]. http://www.cs.cmu.edu/~kangli/code/Image_Stabilizer.html.

Lingg L, Rottenberg S, Francica P. Meiotic genes and DNA double strand break repair in cancer. Front Genet. 2022;13:831620. doi:10.3389/fgene.2022.831620.

Longtine MS, McKenzie A, Demarini DJ, Shah NG, Wach A, Brachat A, Philippsen P, Pringle JR. Additional modules for versatile and economical PCR-based gene deletion and modification in *Saccharomyces cerevisiae*. Yeast. 1998;14(10):953–961. doi:10.1002/(SICI)1097-0061(199807)14:10<953::AID-YEA293>3.0.CO;2-U.

Love MI, Huber W, Anders S. Moderated estimation of fold change and dispersion for RNA-seq data with DESeq2. Genome Biol. 2014;15(12):550. doi:10.1186/s13059-014-0550-8.

Malathi K, Xiao Y, Mitchell AP. Interaction of yeast repressor-activator protein Ume6p with glycogen synthase kinase 3 homolog Rim11p. Mol Cell Biol. 1997;17(12):7230–7236. doi:10.1128/MCB.17.12.7230.

Malathi K, Xiao Y, Mitchell AP. Catalytic roles of yeast GSK3β/shaggy homolog Rim11p in meiotic activation. Genetics. 1999;153(3):1145–1152. doi:10.1093/genetics/153.3.1145.

Mallory MJ, Cooper KF, Strich R. Meiosis-specific destruction of the Ume6p repressor by the Cdc20-directed APC/C. Mol Cell. 2007;27(6):951–961. doi:10.1016/j.molcel.2007.08.019.

Mallory MJ, Law MJ, Sterner DE, Berger SL, Strich R. Gcn5p-dependent acetylation induces degradation of the meiotic transcriptional repressor Ume6p. Mol Biol Cell. 2012;23(9):1609–1617. doi:10.1091/mbc.e11-06-0536.

Mao-Draayer Y, Galbraith AM, Pittman DL, Cool M, Malone RE. Analysis of meiotic recombination pathways in the yeast *Saccharomyces cerevisiae*. Genetics. 1996;144(1):71–86. doi:10.1093/genetics/144.1.71.

Matos J, Lipp JJ, Bogdanova A, Guillot S, Okaz E, Junqueira M, Shevchenko A, Zachariae W. Dbf4-dependent Cdc7 kinase links DNA replication to the segregation of homologous chromosomes in meiosis I. Cell. 2008;135(4):662–678. doi:10.1016/j.cell.2008.10.026.

McFarlane RJ, Wakeman JA. Meiosis-like functions in oncogenesis: a new view of cancer. Cancer Res. 2017;77(21):5712–5716. doi:10.1158/0008-5472.CAN-17-1535.

Mitchell AP. Control of meiotic gene expression in *Saccharomyces cerevisiae*. Microbiol Rev. 1994;58(1):56–70. doi:10.1128/mr.58.1.56-70.1994.

Mitchell AP, Bowdish KS. Selection for early meiotic mutants in yeast. Genetics. 1992;131(1):65–72. doi:10.1093/genetics/131.1.65.

Mootha VK, Lindgren CM, Eriksson K-F, Subramanian A, Sihag S, Lehar J, Puigserver P, Carlsson E, Ridderstråle M, Laurila E, *et al.* PGC-1α-responsive genes involved in oxidative phosphorylation are coordinately downregulated in human diabetes. Nat Genet. 2003;34(3):267–273. doi:10.1038/ng1180.

Moretto F, Wood NE, Chia M, Li C, Luscombe NM, van Werven FJ. Transcription levels of a noncoding RNA orchestrate opposing

regulatory and cell fate outcomes in yeast. Cell Rep. 2021;34(3): 108643. doi:10.1016/j.celrep.2020.108643.

Moretto F, Wood NE, Kelly G, Doncic A, van Werven FJ. A regulatory circuit of two lncRNAs and a master regulator directs cell fate in yeast. Nat Commun. 2018;9(1):780. doi:10.1038/s41467-018-03213-z.

Nachman I, Regev A, Ramanathan S. Dissecting timing variability in yeast meiosis. Cell. 2007;131(3):544–556. doi:10.1016/j.cell.2007.09.044.

Nagaoka SI, Hassold TJ, Hunt PA. Human aneuploidy: mechanisms and new insights into an age-old problem. Nat Rev Genet. 2012; 13(7):493–504. doi:10.1038/nrg3245.

Nishimura K, Fukagawa T, Takisawa H, Kakimoto T, Kanemaki M. An auxin-based degron system for the rapid depletion of proteins in nonplant cells. Nat Methods. 2009;6(12):917–922. doi:10.1038/nmeth.1401.

Okaz E, Argüello-Miranda O, Bogdanova A, Vinod PK, Lipp JJ, Markova Z, Zagoriy I, Novak B, Zachariae W. Meiotic prophase requires proteolysis of M phase regulators mediated by the meiosis-specific APC/CAma1. Cell. 2012;151(3):603–618. doi:10.1016/j.cell.2012.08.044.

Ottoz DSM, Rudolf F, Stelling J. Inducible, tightly regulated and growth condition-independent transcription factor in *Saccharomyces cerevisiae*. Nucleic Acids Res. 2014;42(17):e130. doi:10.1093/nar/gku616.

Padmore R, Cao L, Kleckner N. Temporal comparison of recombination and synaptonemal complex formation during meiosis in S. *cerevisiae*. Cell. 1991;66(6):1239–1256. doi:10.1016/0092-8674(91)90046-2.

Pâques F, Haber JE. Multiple pathways of recombination induced by double-strand breaks in *Saccharomyces cerevisiae*. Microbiol Mol Biol Rev. 1999;63(2):349–404. doi:10.1128/MMBR.63.2.349-404.1999.

Park H-D, Luche RM, Cooper TG. The yeast UME6 gene product is required for transcriptional repression mediated by the CAR1URS1 repressor binding site. Nucleic Acids Res. 1992;20(8):1909–1915. doi:10.1093/nar/20.8.1909.

Pertea M, Kim D, Pertea GM, Leek JT, Salzberg SL. Transcript-level expression analysis of RNA-seq experiments with HISAT, StringTie and Ballgown. Nat Protoc. 2016;11(9):1650–1667. doi:10.1038/nprot.2016.095.

Pnueli L, Edry I, Cohen M, Kassir Y. Glucose and nitrogen regulate the switch from histone deacetylation to acetylation for expression of early meiosis-specific genes in budding yeast. Mol Cell Biol. 2004;24(12):5197–5208. doi:10.1128/MCB.24.12.5197-5208.2004.

Raithatha SA, Vaza S, Islam MT, Greenwood B, Stuart DT. Ume6 acts as a stable platform to coordinate repression and activation of early meiosis-specific genes in *Saccharomyces cerevisiae*. Mol Cell Biol. 2021;41(7):e00378-20. doi:10.1128/MCB.00378-20.

R Core Team. R: *A Language and Environment for Statistical Computing*. Vienna: R Found Stat Comput; 2021. https://www.R-project.org.

Rubin-Bejerano I, Mandel S, Robzyk K, Kassir Y. Induction of meiosis in *Saccharomyces cerevisiae* depends on conversion of the transcriptional represssor Ume6 to a positive regulator by its regulated association with the transcriptional activator Ime1. Mol Cell Biol. 1996;16(5):2518–2526. doi:10.1128/MCB.16.5.2518.

Rundlett SE, Carmen AA, Suka N, Turner BM, Grunstein M. Transcriptional repression by UME6 involves deacetylation of lysine 5 of histone H4 by RPD3. Nature. 1998;392(6678):831–835. doi:10.1038/33952.

Sawyer EM, Joshi PR, Jorgensen V, Yunus J, Berchowitz LE, Ünal E. Developmental regulation of an organelle tether coordinates mitochondrial remodeling in meiosis. J Cell Biol. 2019;218(2): 559–579. doi:10.1083/jcb.201807097.

Schindelin J, Arganda-Carreras I, Frise E, Kaynig V, Longair M, Pietzsch T, Preibisch S, Rueden C, Saalfeld S, Schmid B, *et al.* Fiji: an open-source platform for biological-image analysis. Nat Methods. 2012;9(7):676–682. doi:10.1038/nmeth.2019.

Shah JC, Clancy MJ. IME4, A gene that mediates MAT and nutritional control of meiosis in *Saccharomyces cerevisiae*. Mol Cell Biol. 1992; 12(3):1078–1086. doi:10.1128/mcb.12.3.1078

Smith HE, Driscoll SE, Sia RAL, Yuan HE, Mitchell AP. Genetic evidence for transcriptional activation by the yeast Ime1 gene product. Genetics. 1993;133(4):775–784. doi:10.1093/genetics/133.4.775.

Smith HE, Su SS, Neigeborn L, Driscoll SE, Mitchell AP. Role of IME1 expression in regulation of meiosis in *Saccharomyces cerevisiae*. Mol Cell Biol. 1990;10(12):6103–6113. doi:10.1128/mcb.10.12.6103

Strich R, Slater MR, Esposito RE. Identification of negative regulatory genes that govern the expression of early meiotic genes in yeast. Proc Natl Acad Sci U S A. 1989;86(24):10018–10022. doi:10.1073/pnas.86.24.10018.

Strich R, Surosky RT, Steber C, Dubois E, Messenguy F, Esposito RE. UME6 is a key regulator of nitrogen repression and meiotic development. Genes Dev. 1994;8(7):796–810. doi:10.1101/gad.8.7.796.

Subramanian A, Tamayo P, Mootha VK, Mukherjee S, Ebert BL, Gillette MA, Paulovich A, Pomeroy SL, Golub TR, Lander ES, *et al.* Gene set enrichment analysis: a knowledge-based approach for interpreting genome-wide expression profiles. Proc Natl Acad Sci. 2005;102(43):15545–15550. doi:10.1073/pnas.0506580102.

Tedesco M, La Sala G, Barbagallo F, De Felici M, Farini D. STRA8 shuttles between nucleus and cytoplasm and displays transcriptional activity. J Biol Chem. 2009;284(51):35781–35793. doi:10.1074/jbc.M109.056481.

Thorndike RL. Who belongs in the family? Psychometrika. 1953; 18(4):267–276. doi:10.1007/BF02289263.

Tresenrider A, Morse K, Jorgensen V, Chia M, Liao H, van Werven FJ, Ünal E. Integrated genomic analysis reveals key features of long undecoded transcript isoform-based gene repression. Mol Cell. 2021;81(10):2231–2245.e11. doi:10.1016/j.molcel.2021.03.013.

van Werven FJ, Amon A. Regulation of entry into gametogenesis. Philos Trans R Soc Lond B Biol Sci. 2011;366(1584):3521–3531. doi:10.1098/rstb.2011.0081.

van Werven FJ, Neuert G, Hendrick N, Lardenois A, Buratowski S, van Oudenaarden A, Primig M, Amon A. Transcription of two long noncoding RNAs mediates mating type control of gametogenesis in budding yeast. Cell. 2012;150(6):1170–1181. doi:10.1016/j.cell.2012.06.049.

Vidal M, Strich R, Esposito RE, Gaber RF. RPD1 (SIN3/UME4) is required for maximal activation and repression of diverse yeast genes. Mol Cell Biol. 1991;11(12):6306–6316. doi:10.1128/mcb.11.12.6306

Vidan S, Mitchell AP. Stimulation of yeast meiotic gene expression by the glucose-repressible protein kinase Rim15p. Mol Cell Biol. 1997;17(5):2688–2697. doi:10.1128/MCB.17.5.2688.

Wang H, Clark I, Nicholson PR, Herskowitz I, Stillman DJ. The *Saccharomyces cerevisiae* SIN3 gene, a negative regulator of HO, contains four paired amphipathic helix motifs. Mol Cell Biol. 1990;10(11):5927–5936. doi:10.1128/mcb.10.11.5927-5936.1990

Washburn BK, Esposito RE. Identification of the Sin3-binding site in Ume6 defines a two-step process for conversion of Ume6 from a transcriptional repressor to an activator in yeast. Mol Cell Biol. 2001;21(6):2057–2069. doi:10.1128/MCB.21.6.2057-2069.2001.

Wickham H, Averick M, Bryan J, Chang W, McGowan LD, François R, Grolemund G, Hayes A, Henry L, Hester J, *et al.* Welcome to the tidyverse. J Open Source Softw. 2019;4(43):1686. doi:10.21105/joss.01686.

Williams RM, Primig M, Washburn BK, Winzeler EA, Bellis M, de Menthière CS, Davis RW, Esposito RE. The Ume6 regulon coordinates metabolic and meiotic gene expression in yeast. Proc Natl Acad Sci. 2002;99(21):13431–13436. doi:10.1073/pnas.202495299.

Winter E. The Sum1/Ndt80 transcriptional switch and commitment to meiosis in *Saccharomyces cerevisiae*. Microbiol Mol Biol Rev MMBR. 2012;76(1):1–15. doi:10.1128/MMBR.05010-11.

Xu L, Ajimura M, Padmore R, Klein C, Kleckner N. NDT80, A meiosis-specific gene required for exit from pachytene in *Saccharomyces cerevisiae*. Mol Cell Biol. 1995;15(12):6572–6581. doi:10.1128/MCB.15.12.6572.

Yu G, Wang L-G, Han Y, He Q-Y. Clusterprofiler: an R package for comparing biological themes among gene clusters. OMICS J Integr Biol. 2012;16(5):284–287. doi:10.1089/omi.2011.0118

Editor: C. Kaplan